Electrochimica Acta 275 (2018) 155–171

Contents lists available at ScienceDirect

Electrochimica Acta

journal homepage: www.elsevier.com/locate/electacta

Electrochemical measurements of 1D/2D/3DNi-Co bi-phase mesoporous nanohybrids synthesized using free-template hydrothermal method

O. Guellati [a, b, d, *], A. Harat [a], D. Momodu [c], J. Dangbegnon [c], T. Romero [d], D. Begin [d], C. Pham-Huu [d], N. Manyala [c], M. Guerioune [a]

[a] Laboratoire d'Etude et de Recherche des Etats Condensés (LEREC), Département de Physique, Université Badji-Mokhtar de Annaba, BP. 12, 23000 Annaba, Algeria
[b] Université Mohamed Cherif Messadia de Souk Ahras, Fac. Sci, BP. 1553, 41000 Souk-Ahras, Algeria
[c] Department of Physics, Institute of Applied Materials, SARCHI Chair in Carbon Technology and Materials, University of Pretoria, Pretoria 0028, South Africa
[d] Institut de Chimie et Procédés pour l'Energie, l'Environnement et la Santé (ICPEES) - ECPM - CNRS - UdS, 25 rue Becquerel, 67087 Strasbourg Cedex 2, France

ARTICLE INFO

Article history:
Received 7 October 2017
Received in revised form
8 April 2018
Accepted 16 April 2018
Available online 17 April 2018

Keywords:
Free-template hydrothermal synthesis
Ni-Co bi-phase nanohybrids
Electrochemical supercapacitors
Energy storage

ABSTRACT

In this study, a facile and low cost free-template hydrothermal precipitation method was used to synthesize mesoporous Ni-Co based bimetallic carbonates $(CO_3)^{2-}$ and/or hydroxides $(OH)^-$micro/nanostructures with different morphologies (1D, 2D and 3D) based on variant stoichiometric compositions. The effect of the growth temperature, synthesis time as well as the Ni/Co-precursors ratio on the physico-chemical properties and faradic electrochemical behavior of these products was investigated. The as-obtained bi-phase nanohybrids were characterized extensively structurally and morphologically. The textural analysis results confirmed the presence of mesoporous products with a BET-SSA ~50 $m^2 g^{-1}$ (0.52 $cm^3 g^{-1}$ pore volume) for the 3D urchin-like structure and a BET-SSA ~ 47.14 $m^2 g^{-1}$ (0.31 $cm^3 g^{-1}$ pore volume) was obtained for the 2D nanoflakes structure.

The electrochemical measurements performed in a 6.0 MKOH aqueous electrolyte depicted excellent electrochemical performance ascribed to the optimized composition of Ni-Co LDH (or α-$Ni(OH)_2$) with $Co_2(OH)_3Cl$ and their unique hierarchical mesoporous nanoflake and urchin-like architectures. In addition, an exceptionally notable specific capacitances (capacities) of 1700 F g^{-1} (161 mAh.g^{-1}) and 1379 F g^{-1} (192 mAh.g^{-1}) were obtained for both structures at 5 mV s^{-1} scan rate (0.5 A g^{-1} gravimetric current density) respectively. These are much better than mono - hydroxides synthesized in same conditions with 351 F g^{-1} (90 mAh.g^{-1}) for Ni and 216 F g^{-1} (21.5 mAh.g^{-1}) for Co. A good cyclic stability of ~98% after 2000 charge-discharge cycles at 30 A g^{-1} was recorded depicting their potential as suitable materials for energy storage devices.

1. Introduction

Electroactive material properties such as size, contact surface area and crystallinity have a profound effect on the material performance in numerous applications especially those related to energy storage, catalysis and environment [1–5]. Therefore, more environmentally friendly, faster and energy-efficient synthesis methods for nanoparticle production are currently of interest; especially for transition metal hydroxide nanoparticles.

In recent years, supercapacitors, a promising energy storage and conversion device, has received intense attention due to its high power density, rapid charge/discharge rate and excellent cyclic stability [6]. They are required to operate at high current densities and to have a long cycle life for large scale applications. In particular, electrochemical supercapacitors (ESCs), also known as ultracapacitors, are adopted in computer power back-up systems, hybrid electric vehicles, industrial power plants, military devices, and memory backup systems. They exhibit higher power density

* Corresponding author. Laboratoire d'Etude et de Recherche des Etats Condensés (LEREC), Département de Physique, Université Badji-Mokhtar de Annaba, BP. 12, 23000 Annaba, Algeria.
E-mail address: ouanassa.guellati@univ-annaba.org (O. Guellati).

https://doi.org/10.1016/j.electacta.2018.04.112
0013-4686/

and longer lifespan compared to rechargeable lithium-ion batteries, and higher energy density compared to traditional dielectric capacitors. Typical electroactive materials include carbon-based materials, transition metal oxides and conducting polymers, which reversibly store charge via double-layer capacitance and/or pseudo-capacitance [7]. The development of ESC materials is necessary to improve the energy density of the device without sacrificing the high power density and long cycle life.

Thus, developing the transition metal oxides/hydroxides and carbonate hydroxide nanomaterials, particularly those composed of Ni- and/or Co-which are less expensive replacements for noble electroactive metals, have attracted considerable attention, among researchers in recent years [8–10]. This is because of their earth abundant nature, low cost, environmentally friendly, multiple valence state and high theoretical activity among other faradic materials [11]. Ni–Co alloys are commonly employed as important engineering materials due to their unique properties such as high strength, heat conductivity and electrocatalytic activity [12]. The development and synthesis of smart nanostructures from such materials could be an effective approach towards developing high-performance supercapacitive materials. The controllable synthesis and structural tuning of these materials with desirable composition and hierarchical structure (other than $NiCo(OH)_2$ and $NiCo_2O_4$) are also anticipated to have great potential for electrochemical energy storage. However, there still remains a great challenge to achieving such novel structures with very little studies reported in literature [12–18].

Specifically, layered mono-metal hydroxide like $Co(OH)_2$ and $Ni(OH)_2$ as well as their combination were considered as promising electroactive materials for ESCs system due to their high theoretical specific capacitance and well defined electrochemical properties [19]. Unfortunately, their relatively low conductivity and limited surface area restricts their further application. Therefore, much effort has been devoted by some scholars in preparing much better conducting Ni-Co based hydroxide and oxide nanomaterials with various morphologies, including nanoparticles, nano-needles, nanowires, nanosheets and nanoflakes [11]. Besides, the alternative routes employed to improve the activity of the mono-hydroxide are rather limited. Therefore, mixed hydroxides are often used to modulate the electrode properties through synergistic effects arising from the intimate electronic interaction of the components [20]. It has been shown that the addition of cobalt to nickel oxide/hydroxide enhances the electrochemical performance of the electrodes [21] and the main reason for incorporating the cobalt is to increase the material electrode's conductivity.

Based on the earlier ideas postulated by researchers on designing and developing electrode materials with reasonable electrochemical properties, we report the successful synthesis of bimetallic (Ni-Co) based carbonate $(CO_3)^{2-}$ and/or hydroxide $(OH)^-$micro/nanostructures using a free-template one-step hydrothermal method with urea, depicting a simple, efficient and low cost growth route [22,23]. We also studied the effect of varying the principal parameters (growth temperature, synthesis time as well as the Ni/Co-precursors ratio) on the formation of different kind of electroactive morphologies such as urchin-like, nanofiber or nanosheet forms corresponding to 1D, 2D and 3D structures respectively. Consequently, the electrochemical measurements have been carried out on these new bi-phase nanohybrids to display the effect of the electroactive materials morphology on the device performance. Despite the versatile methods reported, fabrication of the nanostructured materials with desirable morphology and composition still remains a big challenge and great interest in the field of material science. Moreover, to the best of our knowledge, the systematic preparation of mesoporous Ni-Co carbonate and/or hydroxide multi-phase nanostructures with varying Ni-Co ratio for electrochemical measurements has not yet been reported in literature.

2. Experimental procedure

All chemicals, Urea (Merck, purity ≥ 98%), Ni and Co chloride (Sigma-Aldrich, purity ≥ 99.99%), were of analytical grade and were used without further purification. Nickel Foam (NiF) rectangular sheets was procured from Alantum (Munich, Germany) of areal density of 420 g m^{-2} as well as diameter and thickness of 1.6 mm and 0.2 mm, respectively.

2.1. Ni-Co carbonate and/or hydroxide based bi-phase nanocomposites synthesis

0.1 M Nickel (II) chloride hexahydrate ($NiCl_2 \cdot 6H_2O$) and 0.1 M Cobalt (II) chloride hexahydrate ($CoCl_2 \cdot 6H_2O$) were dissolved in deionized water for 10 min at room temperature. After that, 0.5 M urea (CH_4N_2O), which is highly soluble in water, was added into the above mixture and ultrasonicated for 30 min until a dark pink transparent solution was obtained which was transferred into a 40 mL Teflon-lined hydrothermal autoclave system. The autoclave was sealed, maintained at two different growth temperatures (120 and 180 °C) during two different times (6 and 18 h) and then allowed to cool down naturally to room temperature. The obtained products with distinct colors were filtered and washed several times with distilled water and ethanol before drying in an oven at 80 °C overnight.

Subsequently, a series of crystalline bi-metallic Ni and Co hydroxide nanohybrids were prepared using a simple, low-cost hydrothermal synthesis procedure by changing the Co precursor molarity (i.e. Ni:Co = 1:1, 1:2 and 1:3). Nonetheless, the concentration of urea and the growth parameters were kept the same. The corresponding samples obtained were designated as Ni-Co **(x h - y °C)** (where x = **duration** time and y = **temperature** of growth).

2.2. Preparation of working electrode from the active materials

The working electrodes for electrochemical performance evaluation of Ni-Co based carbonate and/or hydroxide bi-phase nanohybrid material were prepared as follows: firstly, a mixture containing 80 wt.% of Ni-Co based electroactive materials (Ni-Co bi-phase hydroxide with different stoichiometry), 10 wt.% of carbon black (CB) and 10 wt.% of polyvinylidene difluoride (PVdF) binder with few drops of 1-methyl 2-pyrrolydone (NMP) solvent was well mixed in an agate mortar to form a paste. This was spread onto a $1 \times 1\ cm^2$ area of pre-treated NiF (serving as a current collector) and dried at 80 °C in an oven for 24 h to ensure complete evaporation of the NMP.

2.3. Materials characterization

The synthesized materials were extensively characterized in order to mainly study the effect of structure, morphology and elemental composition on the electrochemical behavior. The structural characterization of our Ni-Co carbonate and/or hydroxide based products were investigated by powder X-ray diffraction (XRD) using an XRD D8 ADVANCE-BRUKER AXS diffractometer equipped with a copper anticathode tube "Cu Kα radiation" (λ = 1.5406 Å) and a graphite monochromator rear blade, operating at 40 kV and 40 mA with a scanning rate of $0.2°.s^{-1}$. The XRD patterns of all specimens were recorded in the [10°–90°] 2θ range.

The products' morphology were analyzed using a Field Emission Scanning Electron Microscopy, FE-SEM technique (JEOL 6700-FEG microscope) operating at 3 kV equipped with an Energy

dispersive X-ray spectroscopy (EDX) component which aided the determination of the chemical composition (quantitative analysis) in order to control the multi-structures quality, purity and dimension. For the FE-SEM analysis, the products were fixed directly on the sample holder by a graphite paste. Prior to all analyses, the samples were covered by a thin layer of carbon in order to avoid the charging effect problems.

Raman spectroscopy measurements was carried out at room temperature with a Horiba Jobin Yvon Lab-RAM Aramis confocal Raman spectrometer equipped with a cooled CCD camera and an automated XYZ table, at laser excitation of 532 nm. Using a filter D2, the laser power energy that reaches the samples is 0.33 mW.

Fourier-Transform Infra-red (FTIR) spectra of these Ni-Co carbonate and/or hydroxide based nanocomposites were recorded using a Bruker Vertex 77v spectrometer in the 400 to 4000 cm^{-1} wave number range with 4 cm^{-1} resolution and analyzed with an Opus software.

The thermal stability of the bi-phase nanohybrids were measured using a Thermo Gravimetric Analysis technique, which was carried out using TA Instruments Q600 Simultaneous (DSC/TG) analyzer through which measurements of the weight change in the material as a function of temperature were observed in 20 sccm N_2-gas flow. The temperature was increased from room temperature to 1000 °C with a heating rate of 10 °C.min^{-1}.

The Brunauer–Emmett–Teller (BET) specific surface area measurements and the pore size distribution of the as-synthesized Ni-Co based samples were carried out on a Tristar (Micromeritics, ASAP 2420) system using N_2 as the adsorbent in liquid nitrogen temperature. The BET SSA and pore sizes were calculated from the N_2 adsorption/desorption isotherms and the Barrett–Joyner–Halenda (BJH) method respectively. Before measurements, the samples were initially de-gassed over night under vacuum at room temperature to avoid products transformation and also to remove impurities and moisture.

2.4. Electrochemical measurements

The electrochemical measurements were carried out using a Bio-logic "VMP-300 potentiostat" (Knoxville TN 37930, USA), electrochemical workstation "controlled by an EC-Lab® V10.37 software", under ambient temperature in a three-electrode cell setup using 6.0 M KOH aqueous electrolyte with a glassy carbon counter electrode and a Ag/AgCl (3 M KCl) reference electrode.

The cyclic voltammetry (CV) tests were carried out in the potential range − 0.2–0.5 V at increasing scan rates ranging from 5 to 100 mV s^{-1}. For the chrono-potentiometry (CP) tests, they were also carried out for different current density ranging from 1 to 100 A g^{-1}. Finally, electrochemical impedance spectroscopy (EIS) measurements were conducted in the frequency range 0.01 Hz–100 kHz with an open circuit potential in order to analyze the electrochemical characteristics of the electrode materials at various frequencies as well as to determine its internal resistance and charge transfer resistance.

Additionally, a quantitative evaluation of the electrochemical performance for the as-synthesized mesoporous nanohybrid was done using the formula for gravimetric specific capacitance (C_s in F.g^{-1}) and specific capacity (Q_s in mAh.g^{-1}) derived from CV and CP curves, respectively, according to the following equations [7,24]:

$$(\text{from CV curve}):\ C_s = \frac{\int I\,dV}{m\,\nu\,\Delta V} \tag{1}$$

where m is the mass of the loaded active material (in g), ν represents the scan rate (in mV.s^{-1}), ΔV ($V_c - V_a$) refer to the potential window between high and low potential limit of the CV curve, $\int IdV$ is the integrated area under the curve for the cathodic current of the CV curve (in mA.V).

$$(\text{from CP curve}):\ Q_s = \frac{i\,\Delta t}{3.6} \tag{2}$$

where $i = \frac{I}{m}$ and Δt are the current density and discharge time, respectively.

3. Results and discussion

3.1. Physico-chemical characterization

In order to determine the optimum growth condition for the best stoichiometric composition and the interesting design of active materials, a series of experiments were performed at two different growth temperatures and times with three different (Ni:Co) precursors ratio (1:1, 1:2 and 1:3). Fig. 1 (a, c and e) shows the crystallographic identification XRD spectra of obtained products with different bi-structure nanocomposites based of Ni and Co which were attributed to either hydroxide or carbonate hydroxide in hydrotalcite or brucite configuration depending to the growth conditions (see Fig. 2).

The sharp peaks indicates that the as-synthesized Ni-Co based hydroxide samples illustrate good crystallinity, which can be linked to the unique hydrothermal reaction environment for crystal growth, without additional input from possible impurities indicating also the high purity of the products. Thus, with the equimolar stoichiometry precursors (Ni:Co = 1:1), the main XRD peaks of the products can be assigned to cobalt carbonate hydroxide hydrate (**$Co(CO_3)_{0.5}(OH).0.11H_2O$ -**JCPDS no. 48-0083) with an orthorhombic structure and nickel carbonate hydroxide (**$Ni_2(CO_3)\ (OH)_2$**- JCPDS no. 35-0501) with monoclinic structure at 120 °C and 180 °C for the 6 h synthesis time. However, with the 120 °C/18 h growth condition, the most present phase is **α^*-$Ni(OH)_2.0.75H_2O$**- JCPDS no. 38-0715) as compared to cobalt hydroxide chloride phase (**$Co_2(OH)_3Cl$**- JCPDS no. 01-073-2134) with rhombohedral structure.

With increasing Co molarity, as in the case of Ni:Co = 1:2, for 180 °C during 6 h and for 120 °C during 18 h, the diffraction peak scan be easily indexed to hexagonal NiCo hydrotalcite like- LDH phase (**$Ni_{0.75}Co_{0.25}(CO_3)_{0.125}(OH)_2.0.38H_2O$**- JCPDS No. 40-0216) and Co based phase (**$Co_2(OH)_3Cl$**). When the heating - time reaches 180 °C - 18 h, we can see that the main peaks of (**$Co_2(OH)_3Cl$**) with the presence of β-nickel hydroxide phase (**β- $Ni(OH)_2$** - JCPDS no. 14-0117) exist in an hexagonal structure.

In the case of Ni:Co = 1:3, at 180 °C and for both duration 6 h and 18 h, a mixed phase of dominate nickel carbonate hydrate (**$Ni(CO_3)\cdot 6H_2O$**- JCPDS No. 12-0276) with monoclinic structure and cobalt carbonate hydroxide hydrate (**$Co(CO_3)_{0.5}(OH).0.11H_2O$**) have been formed; whereas for the 120 °C/6 h temperature and synthesis time, a cobalt hydroxide (**$Co_2(OH)_3Cl$**) product has been formed with a **$Ni(CO_3)\cdot 6H_2O$** phase present.

Consequently, from the XRD spectra analysis, the successful fabrication of Ni-Co bi-phase nanostructured materials in layered crystals based on carbonates and/or hydroxides has been demonstrated depending on the growth temperature and time as well as the precursor ratio.

Simply put, the growth mechanism involves a hydrolysis-precipitation process in which urea, (serving as a precipitating agent), can slowly provide both carbonate and/or hydroxyl anions to form the Ni or Co brucite and/or hydrotacite LDH. These results suggest that the growth temperature and synthesis duration play a key role in the progress of the main reactions in the system which

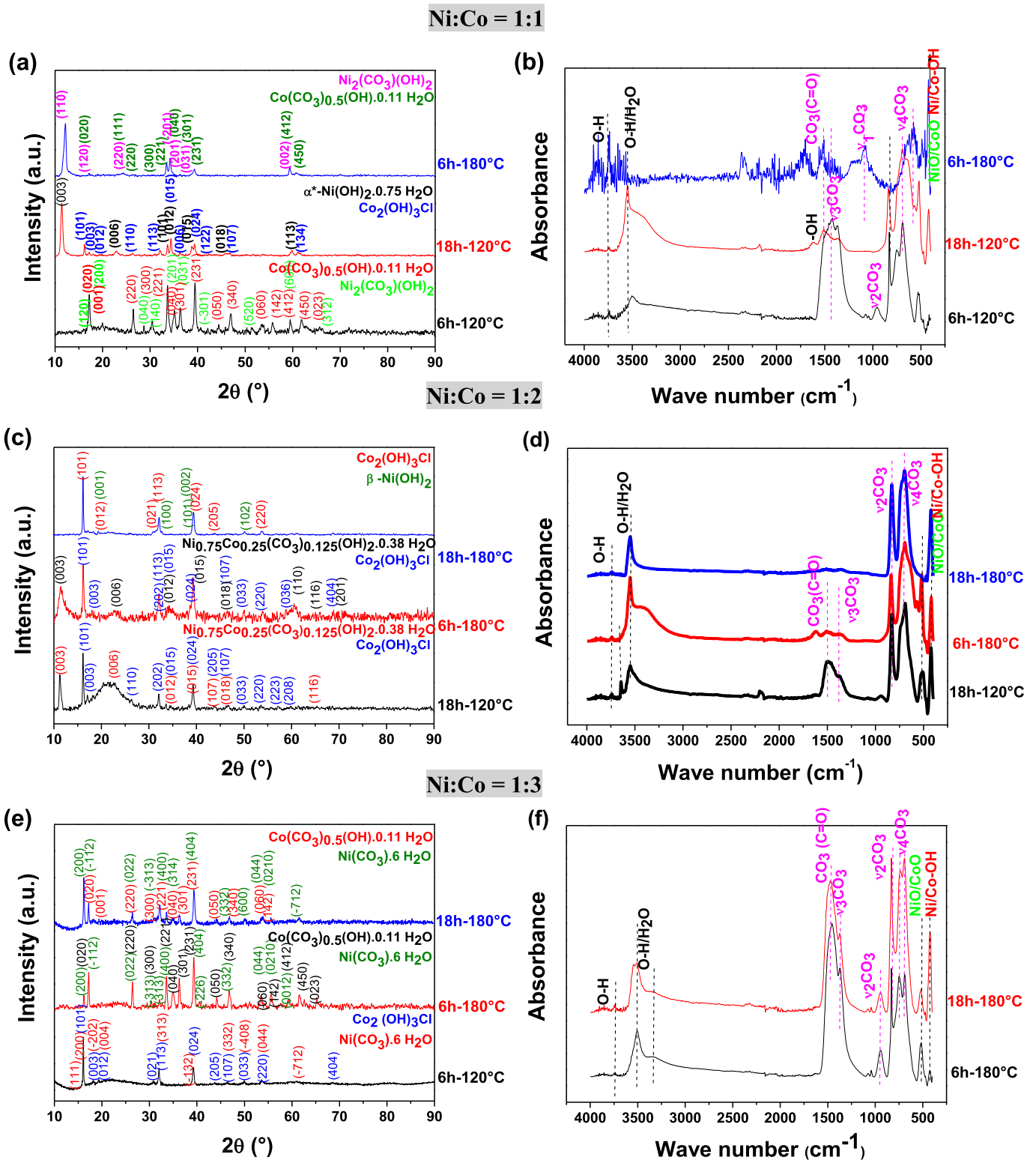

Fig. 1. XRD (a, c, e) and FTIR (b, d, f) spectra of bi-phase products synthesized using urea based hydrothermal method at different conditions for three different precursor stoichiometries.

can be expressed as follows [25]:

$$H_2NCONH_2 + H_2O \rightarrow 2NH_3 + CO_2 \quad (3)$$

$$CO_2 + H_2O \rightarrow CO_3^{2-} + 2H^+ \quad (4)$$

$$NH_3 + H_2O \rightarrow NH_4^+ + OH^- \quad (5)$$

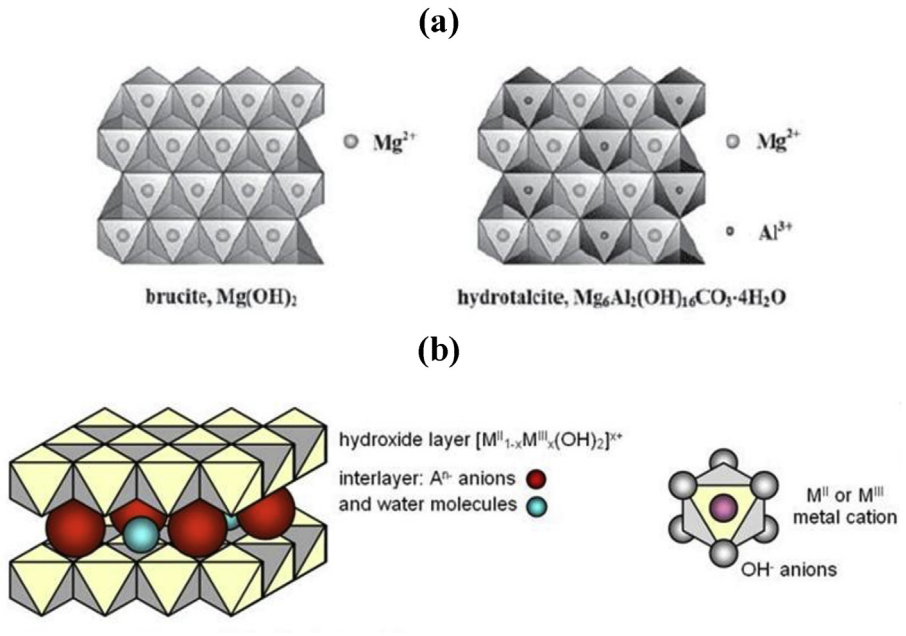

Fig. 2. An example of two different structures: Brucite (hydroxide) and Hydrotalcite (hydrated carbonate hydroxide) (top) and Layered Double Hydroxide "LDH" (down) [17,27].

Generally, mixed transition metal oxides, typically with two different metal cations, have received an upsurge of interest in recent years due to their promising roles in many energy-related applications, such as lithium-ion batteries, supercapacitors, metal–air batteries and fuel cells [3,24,26].

Moreover, the successful preparation of the nanostructures based of Ni-Co carbonate and/or hydroxide is further elucidated by FTIR analysis as shown in Fig. 1 (b, d, e) which reveals some information about the composition and precisely the nature of the chemical bonding. Principally, the incorporation of carbonate (CO_3^{2-}) and $(OH)^-$ions (free or bounded from water molecules) is evident in all FTIR spectra at different positions and with different amount depending on the growth conditions. The interlayer CO_3^{2-} anions may result from the hydrolysis of urea during the synthesis process, as reported above, which aids in dispersing the material precursors.

The narrow common vibration band centered in the range [3740–3750 cm^{-1}] and [3510–3550 cm^{-1}] are assigned to the characteristic peaks of the stretching vibration of hydroxyl groups from hydrogen-bonded to H_2O. While the broad band between 3325 and 3380 cm^{-1} and the band at 3650 cm^{-1} are attributed, respectively, to the stretching mode of adsorbed and/or interlayer water molecules and of -OH groups of the brucite-like structure found with Ni-Co LDH (Ni:Co = 1:2) [28]. Some peaks around 1624 cm^{-1} accompanied the produced Ni-Co hydrotalcite are assigned to the bending mode of structural inter-lamellar physically adsorbed water molecules [15]. The presence of the peaks in the range [1420–1510 cm^{-1}] and [1365 - 1380 cm^{-1}] is observed which are attributed to intercalated CO_3^{2-} anions (C=O groups) and $\nu_3(CO_3)$ vibration band of carbonate anions in D_{3h} planar symmetry, respectively. The $\nu_2(CO_3)$ and $\nu_4(CO_3)$ vibration band are also strongly present around 820 and 690 cm^{-1}, respectively. While, the band around 750 cm^{-1} can be ascribed to the $\nu_4(CO_3)$ bending mode generally obtained with $Co_2CO_3(OH)_2$ or to the O-H bending mode of carboxyl groups as reported in references [29,30]. The two weak bands centered around 950 (ν_2) and 1040 (ν_1) can be attributed to the characteristics of carbonate ions which are present with structure with more Co and more Ni, respectively. Other absorption bands below 1000 cm^{-1} are associated with metal oxide/hydroxide (M–O/M – OH) stretching and bending vibration modes respectively [31]. Additionally, the absorption band which appears at 420, 480 and 520 cm^{-1} in the low wave number region can be assigned to the banding Ni-OH/Co-OH and stretching Ni-O/Co-O vibrations [15]. Thus, the FTIR results confirm the production of Ni-Co carbonate hydroxide based nanostructured materials which are in agreement with XRD results.

The Raman vibrational response measured at room temperature as illustrated in Fig. 3 in the range of 100–1400 cm^{-1}. Only a limited number of Raman studies have been reported until now on the interlayer carbonate or hydroxide anion in hydrotalcite crystals. In this study, the feature peaks corresponding to the Ni-Co carbonate and/or hydroxide based nanocomposite products are in accordance with those reported in other related studies [14,32,33].

Fig. 3 shows the Raman spectra of the bi-phase nanostructured hybrid material with different phase ratio where basically three dominant Raman peaks appear in the 340 -380 cm^{-1} range, 430–450 cm^{-1} range and 520–540 cm^{-1} range which are assigned to the E-type vibration of the Ni-OH lattice, Ni-O stretching (ν NiO) and Co-O symmetric stretching vibrational modes respectively. Furthermore, as reported by Palmer *et* al. [34], the bands with lower wave number below 250 cm^{-1} are attributed to the M – O bonds, lattice vibrations and hydrogen bonds. The strong band situated in the 140-170 cm^{-1} range may be attributed to O–Ni–O bending modes.Whereas, the samples with dominant Co carbonate phase display an intense Raman band at around 1089 cm^{-1} which is assigned to the ν_1 symmetric stretching mode of carbonate groups, hydrogen bonded to the cationic surface of the brucite-like layers and to the hydroxyl deformation mode for 1046 cm^{-1}. Lower intensity Raman band at around 1380 cm^{-1}can be attributed to the anti symmetric stretching vibrations.

In addition, analysis was also done by comparing the as-obtained spectra to the RRuff database with characteristic Raman peaks of $CoCO_3$ seen to be present at wave numbers of 190, 200, 300, 725 and 1090 cm^{-1} (**RRUFF ID:**R140338); $NiCO_3 \cdot 6H_2O$ at 450, 510, 610, 810, 950 and 1090 cm^{-1} (**RRUFF ID:**R061050) and $Ni_2CO_3(OH)_2 \cdot H_2O$ at 210, 380, 440, 510, 680 and 1090 cm^{-1} (**RRUFF**

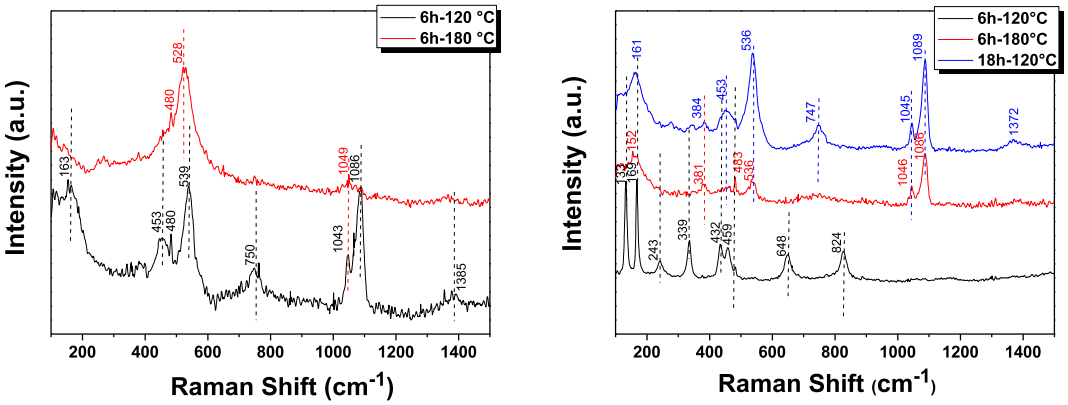

Fig. 3. Raman spectra of some obtained Ni - Co based bi-hydroxide nanocomposites synthesized at different conditions with Ni:Co = 1:1 (left) and 1:3 (right).

ID:R060384). For the hydrotalcite and brucite phase generally, they were situated at 450, 550, 690, 980, 1050 and 1100 cm^{-1} (**RRUFF ID:**R050457/R060527) and at 270, 440, 600, 710, 810 and 1090 cm^{-1} (**RRUFF ID:**R040077), respectively. Thus, it is conclusive to state that a structural change is seen by detailed Raman spectra analysis of the materials.

The investigation of the thermal decomposition behavior in air of some the Ni-Co based bi-phase nanostructured hybrid material using TG and DTG analyses is shown in Fig. 4. An average net weight loss of between 29 and 33 wt.% in the temperature interval of 90–850 °C. The observed percentage weight losses indicate thermal decomposition of Ni and/or Co carbonate hydroxide. Four distinct regions of weight loss were observed in the TGA curves between 200 and 800 °C and the sample remains stable afterwards, depending on the nanocomposite component phases present. The corresponding weight loss of 3–6 wt.% of the samples with LDH structures (Fig. 4b and c) around 91 °C was attributed to the elimination of water in the products.

Meanwhile, the corresponding 10 wt.% loss between 215 and 250 °C was attributed to the decomposition of carbonate anion

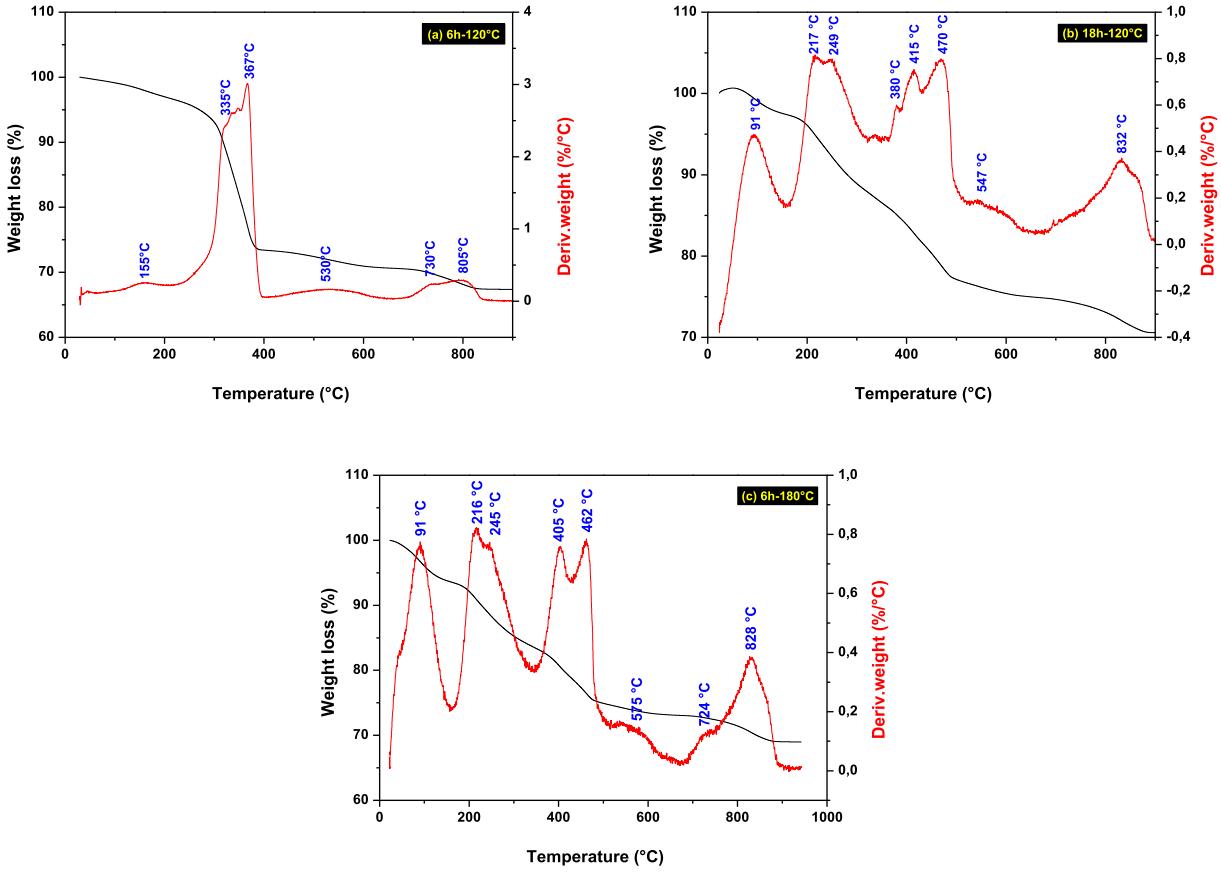

Fig. 4. TGA – DTG analysis results of some obtained Ni-Co based carbonate and/or hydroxides synthesized at different growth conditions with Ni:Co precursors ratios: (a, b) 1:1 and (c) 1:2.

molecules containing the products and physically adsorbed or intercalated water evaporation. The weight loss of 4 wt.% above 800–835 °C is due to the decomposition of the residues.

In general, the thermal stability behavior of all the synthesized samples had a similar profile over the entire temperature range with an initial drop from 180 °C (corresponding to partial dehydroxylation). A strong decomposition peaks (DTG plot) around 380 °C and 450 °C is linked to respective Ni-Co oxides which is in agreement with several investigations previously reported on Ni or Co based carbonate and hydroxide [18,35,36]. Thus, a relatively low calcinations temperature of 400 °C is suitable and sufficient to transform the hydroxides into their corresponding mixed metal oxides as reported in several investigations [37–39].

Remarkably, the decomposition temperature of the Ni-Co based LDH nanostructured hybrid materials (470 °C in Fig. 4b and c) with nanosheets and nanoneedles morphology was higher than that of the Ni-Co mixed carbonate hydroxide with nanorods morphology (370 °C in Fig. 4a) owing to a better thermal stability. The thermal resistance of the as-synthesized nanohybrids was due to the structural composition with more carbonate affected by thermal changes as compared to those with more hydroxides which are generally converted to oxides beyond 400 °C (as seen from the structural characterization results discussed above).

3.2. Morphological characterization

The results from the morphological analysis of the obtained bi-phase nanostructured hybrid materials is revealed using FESEM technique as depicted in Fig. 5 for different hydrothermal growth conditions. The as-synthesized products consist of numerous nanorod-like subunits point in gradually outward like needles, resulting in an urchin-like morphology (for the Ni:Co = 1:1).

In the case of the 6 h/180 °C and 18 h/120 °C synthesis time/temperature, the Ni-Co carbonate hydroxide with a Ni-rich phase, displays some nanoneedles which tend to attach to each other and form large sharp bundles inside the three dimensional (3D) uniform micro-flowers in the form of microspheres with an average diameter of 13 μm. For the nanorods obtained with 6 h/120 °C, they have small diameter of about 50 nm, and the length is close to the radius of the hierarchical microparticles.

Such unique hierarchical micro/nanostructured bimetallic carbonate and/or hydroxide could inherit the advantages from the nanoscale building blocks, while the secondary architecture, typically in micrometer or sub-micrometer dimensions, would bring additional benefits, such as an improved stability, a uniform porosity and a resistance to aggregation. Moreover, these morphologies show good crystallinity and thermal stability proved by their XRD andTGA results earlier discussed.

Likewise, increasing the Co content by two and three folds led to a morphological change of the final products. The final product changed from flower-to hierarchical sheet-like structures consisting of uniform quasi-rectangular nanosheets with a Co-rich phase (see Fig. 5d and e).

The quasi-rectangular nanosheets had an average width and thickness of about 300 nm and 12.5 nm, respectively with pointed plate-like structures for the 1:2 and 1:3 Ni/Co molar ratios.

These morphological results also confirm clearly that the urea plays a crucial role in the formation of the bi-phase structure.

Such porous and hollow 3D structures would greatly benefit the electrode performance in electrochemical applications by offering a high specific surface area, short ionic/electronic diffusion length and efficient channels for mass transport. Thus, aiding in the design of advanced electrode architectures with remarkable chemical composition will be beneficial to boost the supercapacitors device performance.

3.3. Textural characterization

The textural property of the as-synthesized bi-phase nanostructured material was also studied for the 2D and 3D architectures using BET technique. The N_2 adsorption–desorption isotherms (see Fig. 6a and c) can be described as a combination of type I and type IV isotherms. Typically, type IV isotherms were observed for most synthesized samples with an apparent hysteresis loop indicating the presence of a mesopores with a few micropores and macropores. A distinct H3 hysteresis loop was observed in the P/P_0 region of 0.60–0.95, demonstrating further that mesopores are present in both samples and the nanoneedles tend to accumulate to form soft holes. The hysteresis loops in the isotherms linked to the samples with 6h–180 °C and 18h-120 °C synthesis time-temperatures, suggest the presence of mesopores [2–50 nm], as further shown in their Barrett–Joyner–Halenda (BJH) pore size distribution curves (Fig. 6d–f). The mesopores mainly originate from the aggregation in sharp bundles of primary nanoparticles within the nanoneedles-like subunits, while the some of the large mesopores and macropores might be linked to the void spaces between the nanorod and micro-flowers subunits.

Table 1 summarizes the physico-chemical characteristics of the obtained bi-phase nanostructured hybrid materials as Ni/Co quantitative ratio, pore volume and size, their specific surface area. It is worth noting that the BET specific surface area increases generally as the synthesis temperature and synthesis time increases. The relatively high BET values were attributed to the micro-urchin-like morphology observed from FESEM micrographs with important pore volume and size, corresponding to the void spaces between nanoneedles and nanorods component nanocomposites, which will facilitate ion diffusion at the electrode-electrolyte interface during electrochemical device testing.

Specifically, the growth condition significantly increases the amount of mesopores, although much more macropores with size over 100 nm are equally produced. It is well known that mesopores, found in these two cases (1:1 and 1:2), play critical roles in the electrochemical process, due to their capability of facilitating mass ion diffusion and transport and ensure a high electroactive surface area.

Hence, the different porous textures of the three sets of samples with different precursor ratio are likely to depict varying electrochemical performance in this regard. From the BET SSA, the NiCo-hydrotalcite materials with a Ni/Co ratio of 1:3 showed the lowest specific surface area which was obvious from the particle aggregation seen in the FESEM images.

3.4. Electrochemical measurement

For potential application in the energy storage field, electrochemical (EC) measurements were carried out using a three electrode cell set-up with 6MKOH aqueous electrolyte. The electrochemical capacitive performance of nanohybrid based supercapacitors relies not only on the exploitation of high-capacity active materials but also on the rational design of superior electrode architectures. In particular, hierarchical structures, which have uniform assemblies of nanoscale primary building blocks, such as nanoneedles, nanorods, nanoplates and nanosheets, have drawn special interest over the last couple of years due to their exceptional properties and remarkable potential in many fields [2]. Herein, a novel supercapacitor electrode comprising 1D/2D/3D hierarchical Ni-Co based bi-phase nanohybrids (Ni and/or Co based carbonate and/or hydroxide as LDH configuration [40]) with relatively high specific surface area and mesoporous distribution will be successfully studied in order to identify their EC properties for energy storage devices.

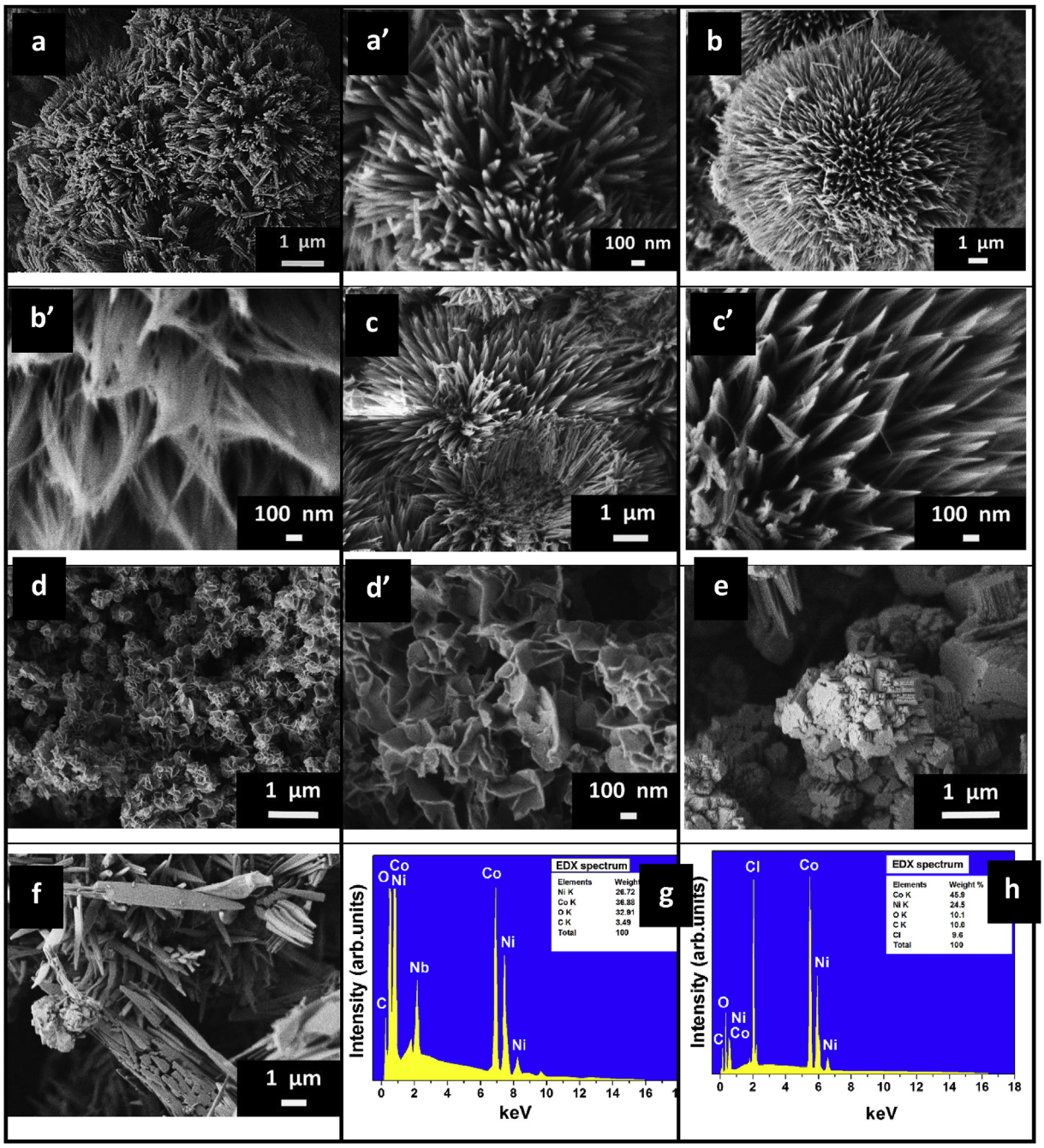

Fig. 5. FESEM micrographs of obtained micro-nanostructures based of Ni-Co bi-phase nanocomposites at different growth conditions and with different Ni:Co precursors ratio: (**a.a'):** 1:1/6h-120 °C, (**b.b'):** 1:1/18h-120 °C, (**c.c'):** 1:1/6h-180 °C); (**d.d'):** 1:2/6h-180 °C, (**e):** 1:3/6h-120 °C, (**f):** 18h-180 °C, EDX (**g**) 18h-120 °C (1:1) and (**h**) 6h-180 °C (1:2).

Cyclic voltammetry (CV) is considered as an important method in supercapacitor to evaluate the potential possibility, the EC behavior and the specific capacitance of electroactive materials used for capacitive deionization.

Fig. 7 shows the CV voltammogram curves of the bi-phase nanohybrid products synthesized at different hydrothermal conditions as electroactive material based electrode at various scan rates ranging from 5 mV s^{-1} to 100 mV s^{-1}.

Notably, a couple of a well-defined intense redox peaks were observed in large window potential generally from −0.2 - 0.5 V (vs. Ag/AgCl) in all the scan rates range, indicating that the EC capacitance of these electrodes mainly results from faradaic redox behavior, which is remarkably different from the closely ideal rectangular CV shape for an electric double-layer capacitor (EDLC) [6]. Generally, two to three pairs of broad and poorly defined redox peaks are related to M−O/M−O−OH, where M refers in our case to Ni or Co [26]. The peak broadening is possibly due to the fact that multiple phases exist and may display broadened redox features.

These obtained strong peaks can be probably attributed to the OH^- associated redox reactions given in the following equations depending to bi-phase nanohybrids composition [18,24,41]:

$$Ni(OH)_2 + (OH)^- \leftrightarrow NiOOH + H_2O + e^- \quad (6)$$

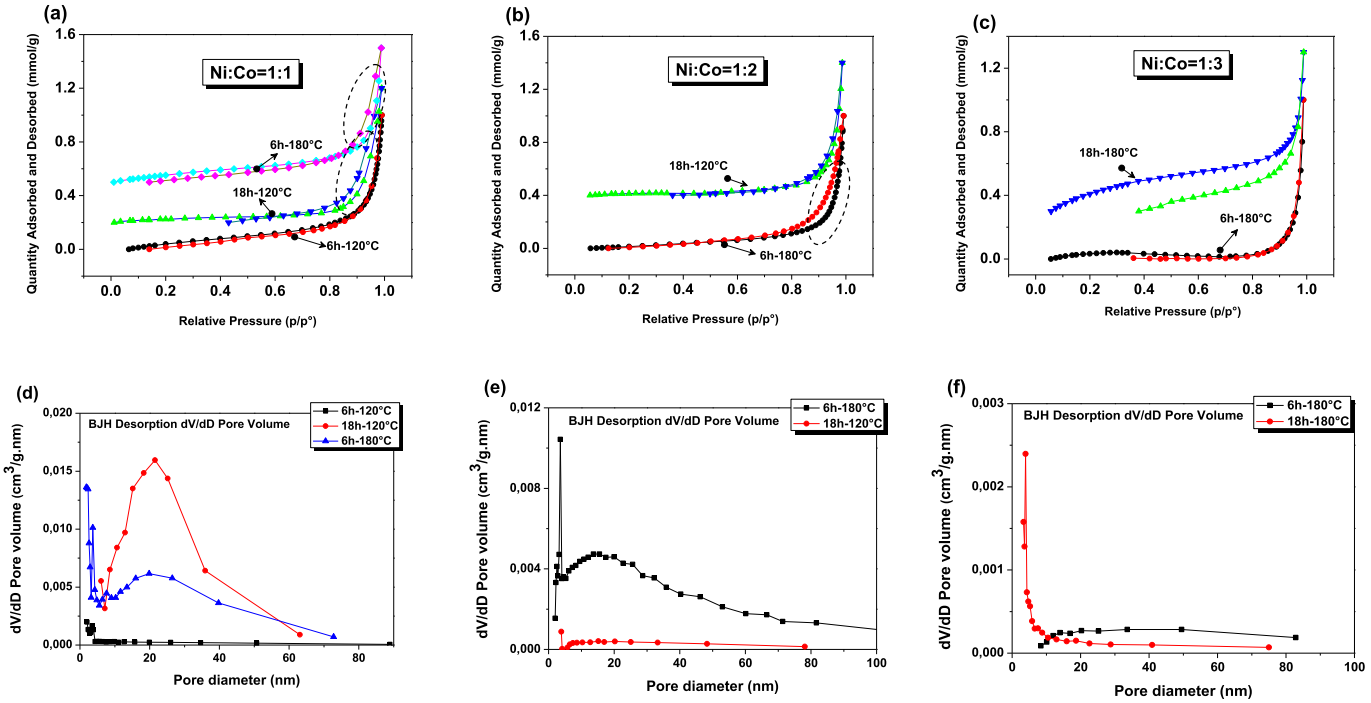

Fig. 6. N_2 adsorption–desorption isotherms (**a-c**) and their corresponding pore size distributions (**d-f**) of the synthesized Ni-Co bi-hydroxide phase nanocomposites.

Table 1
Physico-chemical properties of best products formed at various Ni/Co molar ratio.

Co/Ni molar ratio in the reactants		Crystal phase	BET specific surface area ($m^2\ g^{-1}$)	BJH pore volume ($cm^3\ g^{-1}$)[a]	Pore width (nm)[b]
1:1	6 h/120 °C	$Co(CO_3)_{0.5}(OH).0.11H_2O$ $Ni_2(CO_3)\ (OH)_2$	9.45	0.03	10.46
	18h-120 °C	α^*-$Ni(OH)_2.0.75H_2O$ $Co_2(OH)_3Cl$	**50.59**	**0.52**	**33.91**
	6h-180 °C	$Ni_2(CO_3)\ (OH)_2$ $Co(CO_3)_{0.5}(OH).0.11H_2O$	**85.56**	**0.35**	**15.05**
1:2	18h-120 °C	$Ni_{0.75}Co_{0.25}(CO_3)_{0.125}(OH)_2.0.38H_2O$ $Co_2(OH)_3Cl$	6.14	0.03	30.47
	6h-180 °C	–	**47.14**	**0.31**	**24.47**
1:3	6h-180 °C	$Co(CO_3)_{0.5}(OH).0.11H_2O$ $Ni(CO_3)\cdot 6H_2O$	9.10	0.04	19.98
	18h-180 °C	–	11.61	0.02	10.97

[a] BJH Adsorption cumulative volume of pores between 1.7 nm and 300 nm diameter.
[b] BJH Adsorption average pore width.

$$Co(OH)_2 + (OH)^- \leftrightarrow CoOOH + H_2O + e^- \quad (7)$$

$$CoOOH + (OH)^- \leftrightarrow CoO_2 + H_2O + e^- \quad (8)$$

$$Ni_xCo_{(3-x)}(OH)_6 + 3(OH)^- \leftrightarrow xNiOOH + (3-x)CoOOH + 2H_2O + 3e^- \quad (9)$$

$$Co_2(OH)_3 + (Cl)^- \leftrightarrow 2(CoO_2) + Cl^- + 4H^+ + e^- \quad (10)$$

The oxidation peak close to the upper voltage limit corresponds to the dominant Ni-based phase while the peak at lower potential is for the Co based phase as reported by X. Sun et al. [42] due to the fact that the redox potential of $Co(OH)_2$ to CoOOH transition, is more negative than that of $Ni(OH)_2$ to NiOOH transition. So, comparing these CV curves which correspond to different Ni/Co ratio based bi-phase nanohybrids, the major anodic peak shifts to a more positive potential as Ni content increases in the products, as reported in Ref. [43]. By introducing more Co content into the Ni based system, the redox couples could be shifted to lower potential, preventing the solvent oxidation which induced the performance degradation [42]. This may be attributed to redox process kinetic due to an increase in the ohmic resistance and to the polarization occurring during the faradaic reactions [44]. Consequently, they present rich redox reactions depending on the Ni/Co phase ratio in the nanohybrids structure resulting in a brucite or hydrotalcite configuration [15,25,45–47]. Clearly, we can see also that with increasing scan rate, as shown in Fig. 7 (from 5 to 100 mV s^{-1}), the CV responses have similar shape at different Ni/Co ratio without any slight distortion, in all most curves at high scan rate. These curves show also that the anodic peaks (oxidation) of the electrodes shift positively, while their cathodic peaks (reduction) shift negatively, accompanied with increasing current densities revealing higher charge storage; but this low shifting indicate the excellent

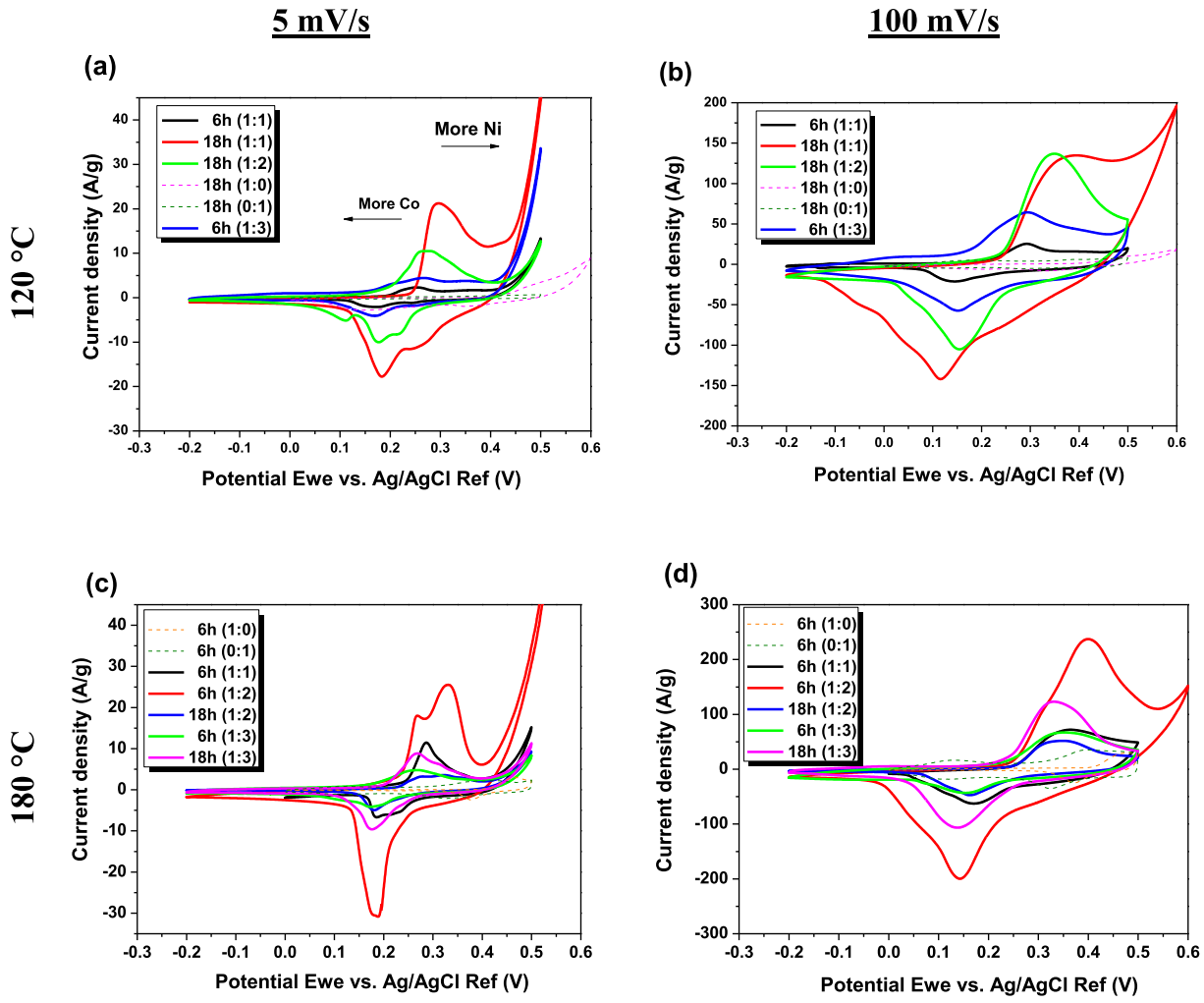

Fig. 7. Cyclic voltammetry comparison at two different scan rates of the synthesized Ni-Co based bi-phase nanohybrids using urea based hydrothermal method.

EC reversibility and outstanding high-rate performance.

Moreover, the enclosed area of the CV plot for the Ni-based material synthesized for 18 h at 120 °C (1:1) and 6 h at 180 °C (1:2) corresponding to α-$Ni(OH)_2$ and NiCo LDH with $Co_2(OH)_3Cl$, respectively, was found to be larger implying its better EC reactivity due to the chemical composition structures and their mesoporous 3D morphology. The good electrochemical response might also be related to the valence and occupation site of the cations in the hydrotalcite structure as well as their specific surface area and pore volume around 50 $m^2\,g^{-1}$ and 0.52 $cm^3\,g^{-1}$, respectively. In addition, the most important result is that the urchins consists of nanoneedle bundles in a fan-like shape, in comparison to the aggregate structure obtained at 6h-180 °C (1:1). This plays a basic role in the morphology requirement for EC accessibility of electrolyte ions within the active material and consequently, a fast diffusion rate within the redox phase.

So, when compared with binary metal oxides (NiO and Co_3O_4) and ternary oxide ($NiCo_2O_4$), bi-metal hydrotalcite structures based on $Ni(OH)_2$ and $Co(OH)_2$ in our results exhibit higher electrical conductivity and improved EC activity in facilitating redox characteristics. This originates from the co-existence of the Ni and Co cation (M^{2+}/M^{3+}) species from within the nanostructured material and the incorporation of anions ($(OH)^-$, $(CO_3)^{2-}$ and Cl^-) and water between the layers as confirmed from previous results [48,49]. These bi-phase heterostructure LDH-based nanohybrid scan provide more electroactive ingredients existing in the interlayer region, making the electron transfer and the intercalation/de-intercalation process of electrolyte ions easier, thus improving their specific capacitances.

The major peak currents I_{pa} and I_{pc} from the cyclic voltammogram are plotted against square root of scan rate, $v^{1/2}$(Randles Sevcik plot) (Fig. 8 a–b) and the redox peak potentials separation ΔE_p (E_{pa}-E_{pc}) is plotted against the scan rate v (Fig. 8 c–d). We found a linear relationship between I_{pa} (or I_{pc}) and $v^{1/2}$in our study which suggests the occurrence of surface reactions and faradaic nature of the products indicating that the energy storage mechanism originate from the surface redox reactions of Ni^{2+}. The linearity further indicates that these electrodes fabricated from the as-synthesized material are diffusion limited, confirmed by the R^2 values around 0.99 [50]. This confirms the postulation that fast kinetics occurs due to the fast rate of charge transfer and ions diffusion. With these very good EC responses, we can confirm that the thin layer and multi-component based structure reduces the ion diffusion distance and enlarges the electrolyte accessible surface area.

In addition, with increasing the scan rates, the separations between the redox peaks are relatively constant at low scan rates and begin to increase at higher ones indicating the limitation arising from charge transfer kinetics [51]. These separations of our electroactive materials can be attributed to the increased Ni hydroxide-like redox behavior exhibited with more Ni content. Noticeably, the

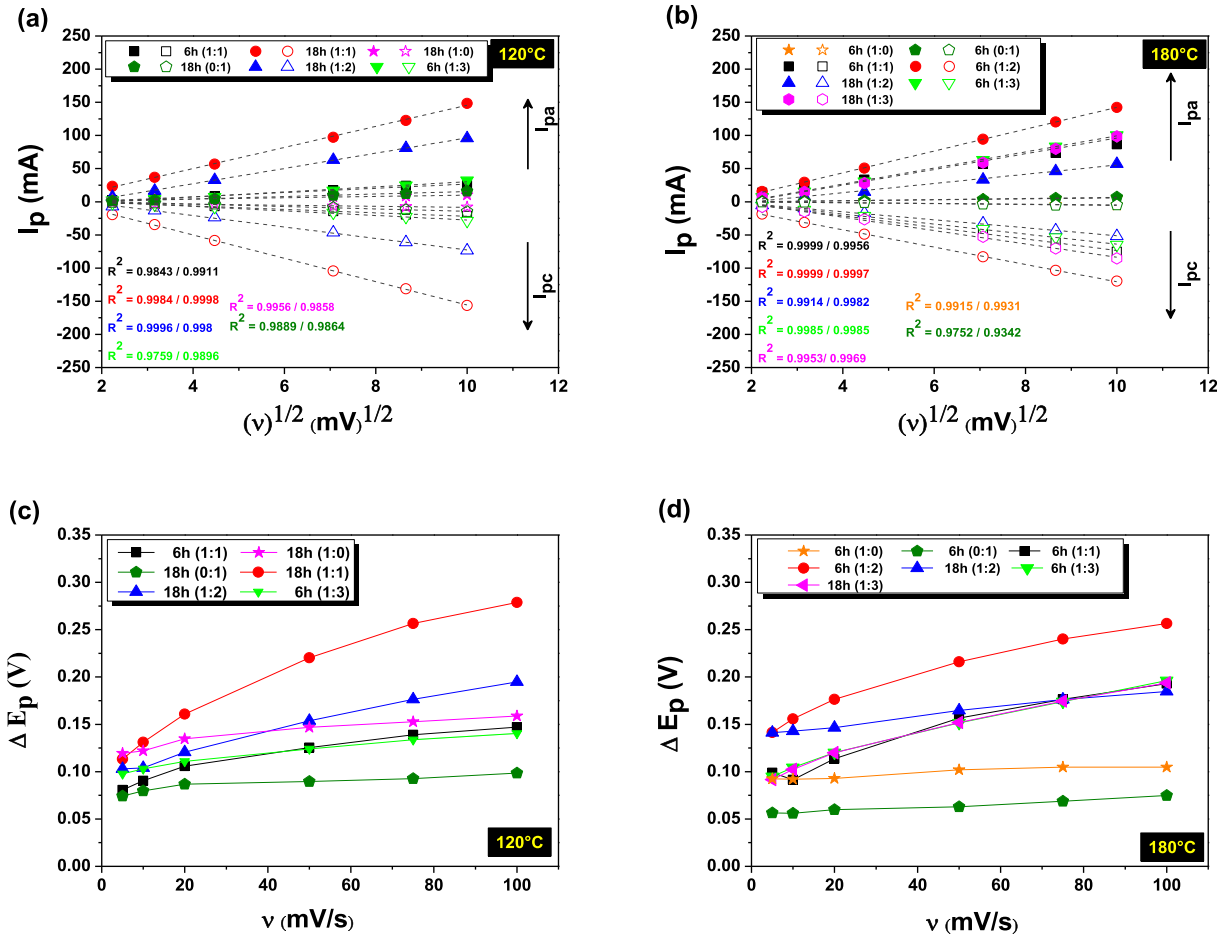

Fig. 8. Current (I_p) vs square root of scan rate (**a, b**) and potential difference (ΔE_p) vs scan rate (**c, d**) of Ni-Co based bi-phase nanohybrid products synthesized at: 120 °C and 180 °C.

potential difference peak-to-peak value found in the range [0.10–0.28 V] was around 0.15, 0.11 and 0.17 V for products synthesized at 18 h-120 °C (1:1), 6 h-180 °C (1:1) and 6 h-180 °C (1:2), respectively, at 20 mV s^{-1}.

Since $n\Delta E_p$ was seen to be greater than 200 mV for the best products, the apparent electron transfer rate constant (k_s) can be estimated (in the case of n ΔE_p> 200 mV at ν > 40 mV s^{-1}) by the following equation as reported in references [51,52]:

$$\log(k_s) = \alpha \log(1-\alpha) + (1-\alpha)\log(\alpha) - \log\left(\frac{RT}{nF\nu}\right) - \left(\frac{\alpha(1-\alpha)nF\Delta E_p}{2,303\,RT}\right) \quad (11)$$

$$k_s = \frac{\alpha\, n\, F\, \nu_c}{RT} = \frac{(1-\alpha)\, n\, F\, \nu_a}{RT} \text{ with } slop_c = \frac{2,3}{\alpha\, n}\frac{RT}{F} \text{ and } slop_a = -\frac{2,3}{(1-\alpha)n}\frac{RT}{F} \quad (12)$$

where n, ΔE_p, α and ν are the number of electrons transferred in the rate determining reaction, the peaks potential separation, cathodic electron transfer coefficient and the scan rate, respectively. *R*, *T* and *F* are gas constant (8.314 J $mol^{-1}{}^{\circ}K^{-1}$), process temperature (298 K) and Faraday constant (96493C mol^{-1}).

The obtained k_s of our best products (18h-120 °C (1:1) and 6h-180 °C (1:2)) are found to be around 69 s^{-1} (83 s^{-1}) and 110 s^{-1} (126 s^{-1}), respectively at cathodic and anodic process, and obviously higher than that obtained by Tao and co-workers [48], indicating that the synthesized bi-phase nanohybrids with more α-$Ni(OH)_2$ and $Co_2(OH)_3Cl$, with their unique hierarchical micro-nanostructure, greatly improve the faradaic redox reaction and the mass transfer. Consequently, the fast electron transfer helps to improve the high current capacitive behavior as shown by Fig. 8 (a–b).

Thus, on the basis of liquid electrolyte reversibility criteria, we can assume that the reaction approaches much better reversibility at low scan rates where small potential difference suggests a higher reversibility with fast electron transfer rate and more active material can be used during charge-discharge process which will confirm their good reversibility of fast charge-discharge response [53].

In order to reinforce our obtained EC results, galvanostatic charge–discharge measurements at various current densities from 1 to 100 A g^{-1} are also performed on these mesoporous Ni-Co based hierarchical bi-phase nanohybrids and their discharge curves are illustrated in Fig. 9 just for two current densities (1 and 30 A g^{-1}). The nonlinear curves with a plateau are consistent with the above CV results which confirm the faradaic mechanism. Further, these measurements clearly show the effect of these products structural properties on the discharge duration which is much longer around 600 s (at 1 A g^{-1}) with bi-phase nanohybrids based of α-$Ni(OH)_2$ or NiCo hydrotalcite LDH with $Co_2(OH)_3Cl$ in comparison with Ni or Co based carbonate hydroxide bi-phase nanohybrids.

The specific capacitances of the as-prepared three series of

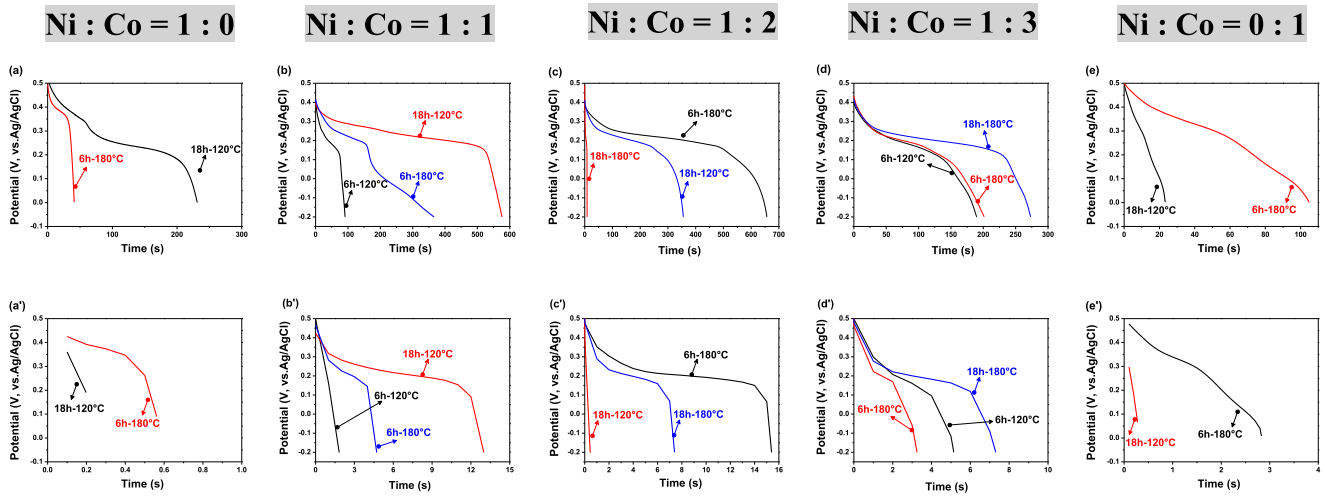

Fig. 9. Discharge curves comparison at two different current densities (a–e) **1 A g^{-1}** and (a'-e') **30 A g^{-1}** of synthesized Ni-Co hydroxide based bi-phase nanohybrids.

products derived from the CV and CD curves are shown in Fig. 10; which steadily decrease with increasing potential scan rates and current densities. Specifically, an exceptionally high specific capacitance (capacity) of 1700 (160 mAh.g^{-1}), 1379 (182 mAh.g^{-1}) and 979 F g^{-1} (54 mAh.g^{-1}) is obtained at a low scan rate of 5 mV s^{-1} (low current density of 1 A g^{-1}) for 18 h-120 °C (1:1), 6 h-180 °C (1:2) and 6 h-120 °C (1:3) corresponding to three different bi-phase nanohybrids as best products, composed of α-Ni(OH)$_2$ hydroxide, NiCo hydrotalcite LDH and Ni(CO$_3$) hydrated carbonate respectively with Co$_2$(OH)$_3$Cl as a second phase.

These obtained specific capacitance at high and low current densities with excellent rate capability are higher than those obtained in previous reports on similar electroactive materials as reported in Table 2.

The capacitance value of the binary Ni–Co sample is higher than that of Ni hydroxide and Co carbonate hydroxide itself using same synthesis route as proved in this work and in other reports [59–62]. Consequently, this improved EC performance is attributed to the binary Co^{2+}/Co^{3+} and Ni^{2+}/Ni^{3+} couples with different percentage (see Fig. 10f) accompanied with specific intercalated ions (as OH^-, Cl^- and CO_3^{2-}) in specific configuration that afford rich faradic capacitance and enhanced conductivity.

As expected, the Q_s decreases gradually with increasing current density due commonly to the limitation of electron/electrolyte transport and of product activation as well as the polarization concentration, resulting in the low utilization of the electroactive materials [29,48].

However, even at high scan rate 100 mV s^{-1} (or at high current density 30 A g^{-1}), these obtained mesoporous hierarchical micro-nanostructures still deliver a remarkable capacitance around 600 F g^{-1} (or capacity up than 120 mAh.g^{-1}) which is quite remarkable. This suggests that about 60% of the capacity is still

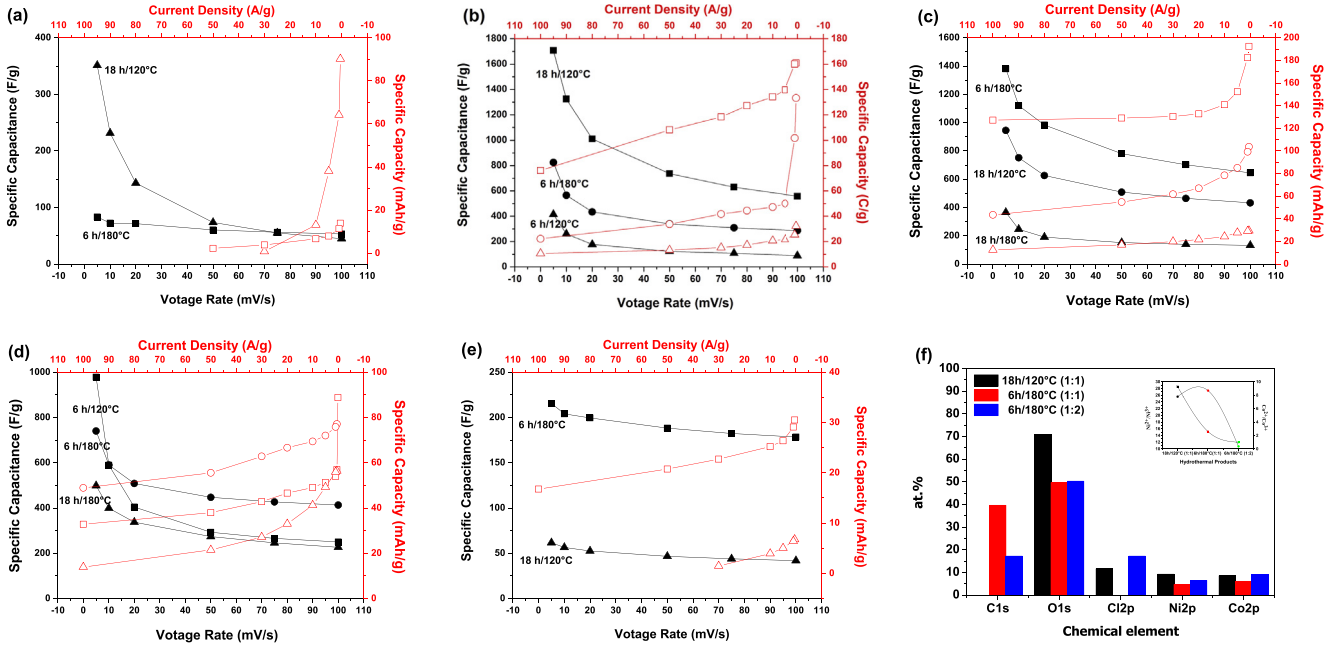

Fig. 10. Specific capacitance (Cs) and capacity (Qs) curves of the synthesized Ni and/or Co hydroxide and/or carbonate based bi-phase nanohybrids for Ni:Co ratio: 1:0 (**a**), 1:1 (**b**), 1:2 (**c**),1:3 (**d**), 0:1 (**e**) and Products element percentage via XPS with their Ni^{2+}/Ni^{3+} ratio (**f**).

Table 2
A comparison of EC properties of transition metal hydroxides-based electrodes evaluated in a three-electrode cell configuration in aqueous alkaline electrolyte found in this work and previously published results.

Synthesis method	Products	Cs ($F.g^{-1}$)	Retention (%) (cycling)	Ref.
Hydrothermal	NiCo LDH $Co_2(OH)_3Cl$	1700 (0.5 A g^{-1})	98% (2000)	This work
	A-$Ni(OH)_2$+$Co_2(OH)_3Cl$	1379		
Precipitation+annealing	$Ni_{0.3}Co_{2.7}O_4$	960 (0.625 A g^{-1})	98.1% (3000)	2013 [26]
Bio-inspired approach	$Co_{0.45}Ni_{0.55}O$/RGO	909.4 (1 A g^{-1})	97% (1000)	2012 [29]
CTAB assisted hydrothermal	$Ni_{0.3}Co_{2.7}O_4$	1423 (1 A g^{-1})	96% (4000)	2015 [44]
Electrostatic assembly	CoAl LDH	547 885	68%	2014 [43]
	CoAl LDH/CNT	(5 mA cm^{-2})	88% (2000)	
One-pot microwave	NiCo LDH/RGO	1622 (5 mV s^{-1})	80% (5000)	2016 [41]
Chemical process	NiCo hydroxide	1030 (3 A g^{-1})	97.3% (1000)	2013 [42]
Microwave	$NiCo_2S$	1110 (5 mV s^{-1})	80% (2000)	2015 [50]
SiO_2 template assisted solvothermal	NiCo LDH	2158.7 (1 A g^{-1})	97.5% (1500)	2015 [49]
Solvothermal	NiAl LDH	1252 (1 A g^{-1})	97% (1000)	2014 [54]
Electro-deposition	CoNi LDH	1201 (1 A g^{-1})	88% (2000)	2016 [55]
Microwave	$Co_{0.2}Ni_{0.8}(OH)_2$	1170 (4 A g^{-1})	94%	2014 [56]
Co-precipitation + oxidation process	CoFe LDH	728 (1 A g^{-1})	65.3% (5000)	2016 [57]
Hydrothermal	$Ni_{1-x}Zn_xS$	1815 (1 A g^{-1})	–	2016 [58]
Hydrothermal	CoAl LDH	550 (1 A g^{-1})	–	2016 [59]
Electrochemical steps	NiCoLDH@Cu foam	1462.5 (1 A g^{-1})	80.46% (2000)	2017 [60]

retained when the current density is increased by 30-fold.

Consequently, we proved that the obtained high specific capacitance of these kind of bi-phase nanohybrids is provided by electroactive sites and significant mesoporous volume in the electrodes indicated in Table 1 above which allows high transport rates of electrolyte ions and electrons simultaneously taking part in the faradaic reactions.

Regarding the cycling stability by subjecting the electrode to repeated charge-discharge steps, as an indispensable factor for electrode material practical use, a good cycling life performance was obtained for the bi-phase nanohybrid electrodes in this study at a high current density by 30 times (see Fig. 11). The average specific capacitance value for the initial cycle is found around 1700 (800 F g^{-1}) and it gradually decreases to 1670 (785 F g^{-1}) after 2000 (1000 cycles), then it remains almost constant during the residual cycles.

Thus, the specific capacitance retention remained at 98% after 2000 cycles, suggesting its excellent cyclic stability and good rate capability provided by robust architecture of the as-synthesized material, charge transfer kinetics and their strong adhesion on

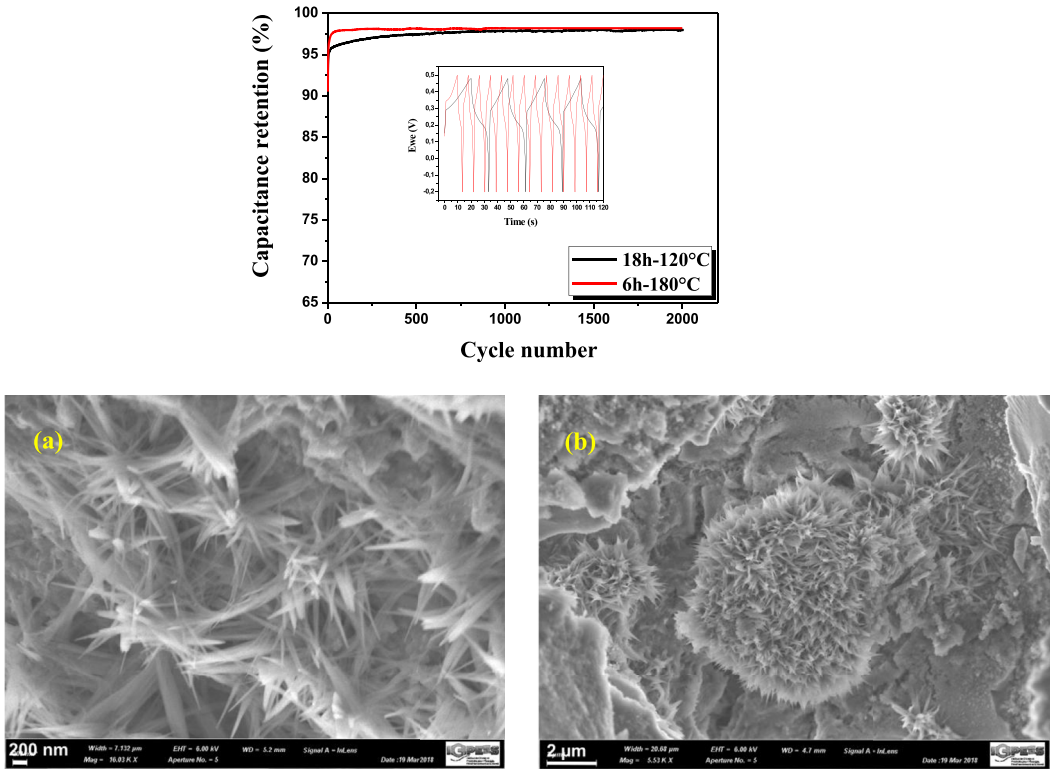

Fig. 11. Capacitance retention as a function of cycle number at a current density 30 A g^{-1} for the best Ni-Co based bi-phase nanohybrids (case Ni:Co = 1:1) and their FESEM micrographs after cycling.

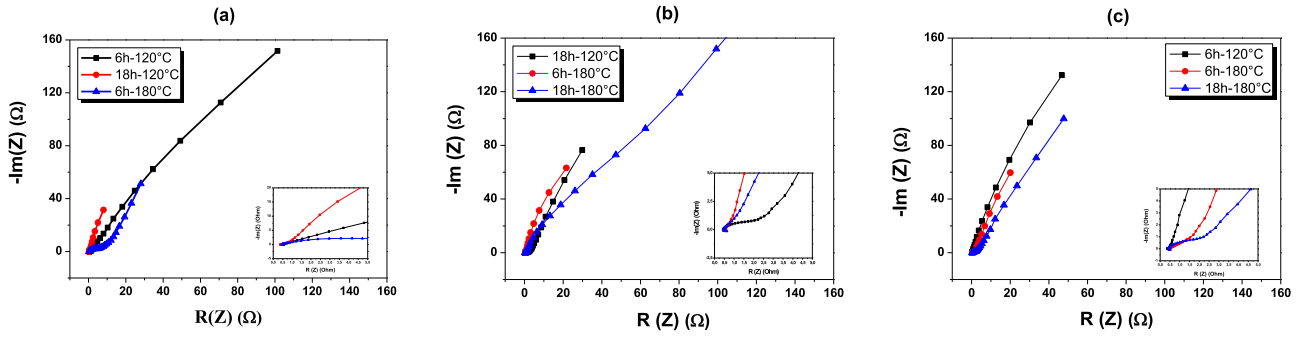

Fig. 12. Nyquist plots of as-prepared Ni-Co hydroxide based bi-phase nanohybrids (inset high frequency region) for Ni:Co: (a) 1:1, (b) 1:2 and(c) 1:3.

the NiF current collector under EC conditions.

For further investigation of the actual Ni-Co bi-phase nanohybrid electrodes, the impedance EIS spectra of obtained sample series were measured in the frequency range from 0.01 to 10^5 Hz in an open circuit potential (E_{oc}), as shown in Fig. 12. Almost all Nyquist plots were characterized by two distinct parts, a partial semicircle at high frequency due to the dispersion effect [61] and a straight deviated line from the imaginary axis at low frequency. This EIS study allows understanding the chemical and physical processes in solutions through charge transfer characteristics at solid-liquid and solid-solid interfaces [44].

The EIS data of best samples were fitted based on an equivalent circuit model using EC-Lab Randomize and Simplex fitting method and the results are illustrated in Fig. 13. The majority of these kind of electroactive materials show smaller semicircle at high frequency region indicating lower interfacial charge transfer resistance demonstrating faster electron transfer process mainly dominated by the pseudo-capacitance from much more α- $Ni(OH)_2$ accompanied with $Co_2(OH)_3Cl$ hydroxides. It is interesting also to note that less deviation (less than 45°) of the sloping line is mentioned below with all products indicating small diffusion resistance and more than quasi ideal pseudocapacitor - faradaic behavior. Therefore, the less ionic flow resistance in the hydroxide based nanohybrid systems causes high specific capacitance confirmed by the above calculated values.

Table 3 summarizes the fitting parameters from these EIS data: $\mathbf{R_s}$ (internal resistance, where the semicircle intersects the real axis, consisting an equivalent series resistance (ESR) of ionic resistance of the electrolyte, intrinsic resistance of the active material and contact resistance at the electroactive material/current collector interface), $\mathbf{R_{CT}}$ (diameter of the semicircle corresponding to the interfacial charge-transfer resistance which is often the limiting factor for the supercapacitor power density), $\mathbf{C_{dl}}$ (double-layer capacitance on the grain surface) and $\boldsymbol{\theta}$ (linear inclination angle in the low frequency region from the ideal capacitive behavior due to the diffusion of electrolyte ions and is usually attributed to a leakage resistance $\mathbf{R_L}$ (or Warburg impedance, **W**) arising from faradaic charge transfer process) [50,62].

As shown in Table 3, R_s values are almost in the range [0.35–0.49 Ω] and are lower with best products which proves the excellent conductivity between current collector, the electroactive bi-phase micro-nanohybrid and the KOH electrolyte.

More importantly, with increasing the Co content in these bi-phase nanohybrids, the R_{CT} values arise but in most are less than the values obtained with different Ni-Co based oxides or hydroxides composition found in the literature [14,29,50,63,64]. However, the R_s and R_{CT} values notably change with increasing or decreasing depending to the nanohybrids composition and morphology after cycling indicating the variation of electron/ion conductivity within the sample after long-term cycling between 1000 and 2000 cycles and consequently one of the main contributing factors in C_s improvement; which is in agreement with the literature.

Finally, we attribute the excellent obtained EC properties to the desirable synergy of these kind of hydroxide based bi-phase nanohybrids chemical composition and design in micro-nanoscale configuration where specifically, the primary nanoneedles based opened bundles provide high EC activity and relatively high active surface area; while the secondary hierarchical micrometer assembly prevents the undesirable agglomeration and ensure the stability of the mesoporous structure. So, we confirm that these 3D micro-nanostructures in flower shape based of opened nanoneedle bundles are more favorable in fast diffusion and OH^- ions penetration for faster EC kinetics and maximum reversible redox process in charge storage. Consequently, the low cost and simple urea based hydrothermal method for the production of hydroxide based bi-phase nanohybrids with different ratio in different morphologies with very promising EC performance.

4. Conclusion

A novel bi-phase nanohybrids based of Ni and/or Co carbonate and/or hydroxide with mesoporous texture in 3D microspheres composed of opened nanoneedle-bundles in fan form or in assembly of 2D nanoflakes were successfully synthesized via a simple and low cost free template urea based hydrothermal method.

We have demonstrated via the EC measurements that the coexistence of two metal species in unique hierarchical micro/nanohetero-metallic bi-phase nanohybrids intercalated with $(CO_3)^{2-}$ anions and some H_2O molecules provides richer redox reaction in aqueous alkaline electrolytes promising EC devices for fast and efficient energy storage in comparison with their corresponding monometallic hydroxide or carbonate hydroxide. Therefore, these EC results have indicated that the unique 3D micro/nano-architecture of α-$Ni(OH)_2$ or Ni-Co LDH with $Co_2(OH)_3Cl$ bi-phase nanohybrids, possesses excellent EC properties as a negative electroactive material, in reversible faradaic system, exhibiting a high capacitance around 1700 $F.g^{-1}$and a high cycling stability (2% loss after 2000 cycles) which is superior than those reported in the literature.

So, the performance of these coupling hydroxide based nanostructured hybrid materials can be ascribed to the following factors: (1) the turbostratically disordered and quasi poorly crystallized structure of the α-phase hydroxides in brucite or hydrotalcite configuration present in the nanostructured hybrid material with high EC activity, (2) ultrathin bundles of nanoneedles and nanoflates based nanoclusters possessing high specific surface area and pore volume which are beneficial for the full contact of the electroactive materials with the electrolyte and (3) the combination

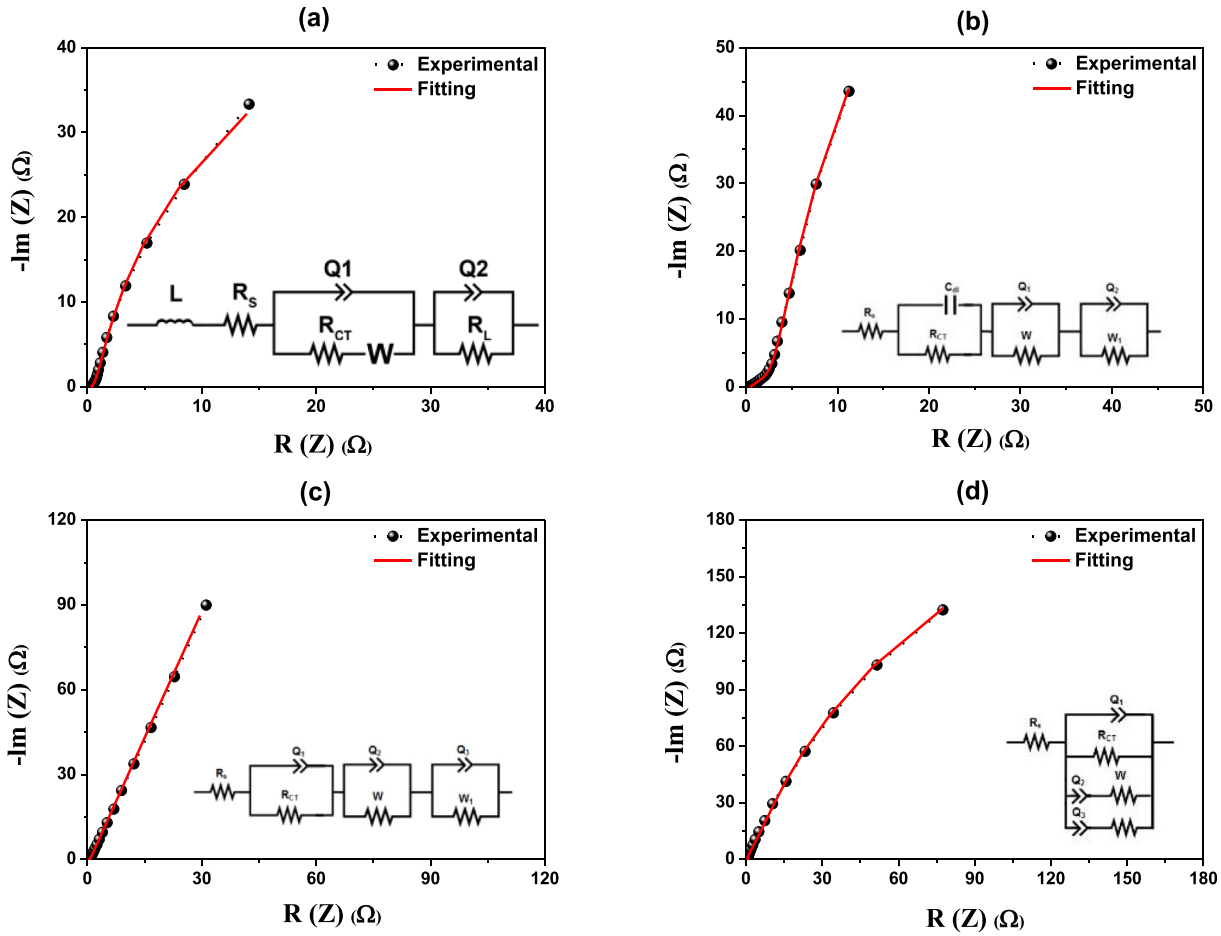

Fig. 13. Fitting results of the Nyquist plot experimental impedance data of the best Ni-Co based bi-phase nanohybrids (inset equivalent circuit model): 18h-120 °C (1:1) (a), 6h-180 °C (1:1) (b), 6h-180 °C (1:2) (c) and 6h-120 °C (1:3) (d).

Table 3
EIS characteristics obtained from the EC-Lab Randomize and Simplex fitting of the experimental impedance data.

Electrode		R_s (Ω)	R_{CT} (Ω)	θ (°)
1:0	18h-120 °C	0.1803 (0.3831)	0.8618 (0.4899)	<45 (= 45)
	6h-180 °C	0.2237 (0.2520)	1.084 (0.9736)	<45 (>45)
1:1	6h-120 °C	0.4423 (0.4747)	0.0333 (0.0457)	37 (34)
	18h-120 °C	**0.3549** (0.3957)	**0.0006** (0.0469)	**29** (16)
	6h-180 °C	0.4640 (0.4856)	1.0180 (7)	15 (20)
1:2	18h-120 °C	0.4479 (0.4483)	0.1021 (0.1267)	39 (21)
	6h-180 °C	**0.4031** (0.3691)	**1.5200** -	**19** (43)
	18h-180 °C	0.4900 (0.4527)	0.4159 (0.3010)	13 (36)
1:3	6h-120 °C	**0.4362** (0.4185)	**0.0279** (0.0125)	**42** (25)
	6h-180 °C	0.4390 (0.4326)	1.9570 (0.0875)	23 (20)
	18h-180 °C	0.4170 (0.4468)	0.1380 (1.9750)	34 (26)
0:1	18h-120 °C	0.3319 (0.3319)	0.6379 (0.4569)	45 (>45)
	6h-180 °C	0.1899 (0.2050)	0.8425 (0.8132)	<45

(in brackets)after stability cycling.

of the contributions from both Ni^{2+} and Co^{2+} ions as well as $(CO_3)^{2-}$, $(OH)^-$or $(Cl)^-$anions in active configuration giving electroactive materials with high-performance EC mechanisms and improved electronic conductivity.

Finally, we proved that these kinds of typical bi-phase nanohybrids with mesoporous texture over large specific surface area and important pore volume can facilitate the electrolyte ion diffusion, enhance the charge transport and provide more electroactive sites for fast electron/ion transfer energy storage. They became one of the most promising electrode materials for supercapacitors as practical electrochemical devices due to its feasible oxidation state, environmental benignity and relatively higher specific capacitance as compared with individual Ni or Co hydroxide.

Acknowledgements

The present work is based on the research supported by the Algeria and South Africa collaboration program between LEREC laboratory, Badji Mokhtar University of Annaba and South African Research Chairs Initiative (SARChI) in Carbon Technology and

Materials of the Department of Science and Technology. The financial support received from National Research Foundation (NRF) and Directorate General for Scientific Research and Technological Development (DGRSDT). The authors would like to acknowledge Th. Romero (IPCEES) and F. Antoni (ICube) for performing, respectively, FESEM and Raman experiment.

References

[1] S. Bashir, J.L. Liu, Nanomaterials and Their Application, Elsevier Inc., 2015, pp. 1–50.
[2] M.R. Lukatskaya, B. Dunn, Y. Gogotsi, Multidimensional materials and device architectures for future hybrid energy storage, Nat. Commun. 7 (2016) 1–13.
[3] Q. Yang, Z. Lu, J. Liu, X. Lei, Z. Chang, L. Luo, X. Sun, Metal oxide and hydroxide nanoarrays: hydrothermal synthesis and applications as supercapacitors and nanocatalysts, Prog. Nat. Sci. Mater. Int. 23 (4) (2013) 351–366.
[4] J. Wang, L. Ji, S. Zuo, Z. Chen, Hierarchically structured 3D integrated electrodes by galvanic replacement reaction for highly efficient water splitting, Adv. Energy Mater. 7 (2017), 1700107–170115.
[5] J. Wang, L. Ji, Z. Chen, In situ rapid formation of a nickel-iron-based electrocatalyst for water oxidation, ACS Catal. 6 (2016) 6987–6992.
[6] G.P. Wang, L. Zhang, J.J. Zhang, A review of electrode materials for electrochemical supercapacitors, Chem. Soc. Rev. 41 (2012) 797–828.
[7] T. Brousse, D. Belanger, J.W. Long, To Be or not to Be pseudocapacitive? J. Electrochem. Soc. 162 (5) (2015) A5185–A5189.
[8] D.S. Hall, D.J. Lockwood, C. Bock, B.R. MacDougall, Nickel hydroxides and related materials: a review of their structures, synthesis and properties, Proc. Math. Phys. Eng. Sci. 471 (2015), 20140792.
[9] K.K. Lee, W.S. Chin, C.H. Sow, Cobalt-based compounds and composites as electrode materials for high-performance electrochemical capacitors, J. Mater. Chem. A 2 (2014) 17212–17248.
[10] Y. Tao, H. Zhu, R. Li, Z. Li, J. Liu, G. Wang, Z. Gu, Microwave synthesis of nickel/cobalt double hydroxide ultrathin flower clusters with three-dimensional structures for high-performance supercapacitors, Electrochim. Acta 111 (2013) 71–79.
[11] C. Yuan, H. Bin Wu, Y. Xie, X.W. Lou, Mixed transition-metal oxides: design, synthesis, and energy-related applications, Angew. Chem. Int. Ed. 53 (2014) 1488–1504.
[12] D.P. Dubal, P. Gomez-Romero, B.R. Sankapal, R. Holze, Nickel cobaltite as an emerging material for supercapacitors: an overview, Nano Energy 11 (2015) 377–399.
[13] Y. Zhu, J. Chen, N. Zhao, W. Lin, C. Lai, Q. Wang, Large-scale synthesis of uniform $NiCo_2O_4$ nanoparticles with supercapacitive properties, Mater. Lett. 160 (2015) 171–174.
[14] X. Cai, X. Shen, L. Ma, Z. Ji, C. Xu, A. Yuan, Solvothermal synthesis of NiCo-layered double hydroxide nanosheets decorated on RGO sheets for high performance supercapacitor, Chem. Eng. J. 268 (2015) 251–259.
[15] L. Xie, Z. Hu, C. Lv, G. Sun, J. Wang, Y. Li, H. He, J. Weng, K. Li, Co_xNi_{1-x} double hydroxide nanoparticles with ultrahigh specific capacitances as supercapacitor electrode materials, Electrochim. Acta 78 (2012) 205–211.
[16] W. Ma, L. Wang, J. Xue, H. Cui, Ultra-large scale synthesis of Co-Ni layered double hydroxides monolayer nanosheets by a solvent-free bottom-up strategy, J. Alloys Compd. 662 (2016) 315–319.
[17] L. Dussault, Etude physico-chimique d'oxydes mixtes issus d'hydroxydes doubles lamellaires. Application à la synthèse de nanofilaments de carbone, Thèse: école doctorale des sciences exactes et de leurs applications, 2005.
[18] V. Gupta, S. Gupta, N. Miura, Potentiostatically deposited nanostructured Co_xNi_{1-x} layered double hydroxides as electrode materials for redox-supercapacitors, J. Power Sources 175 (2008) 680–685.
[19] J.C. Chen, C.T. Hsu, C.C. Hu, Superior capacitive performances of binary nickel-cobalt hydroxide nanonetwork prepared by cathodic deposition, J. Power Sources 253 (2014) 205–213.
[20] W. Zhu, Z. Lu, G. Zhang, X. Lei, Z. Chang, J. Liu, X. Sun, Hierarchical $Ni_{0.25}Co_{0.75}(OH)_2$ nanoarrays for a high-performance supercapacitor electrode prepared by an in situ conversion process, J. Mater. Chem. A 1 (29) (2013) 8327–8331.
[21] J. Han, K.C. Roh, M.R. Jo, Y.M. Kang, A novel co-precipitation method for one-pot fabrication of a Co-Ni multiphase composite electrode and its application in high energy-density pseudocapacitors, Chem. Commun. 49 (2013) 7067–7069.
[22] H. Hayashi, Y. Hakuta, Hydrothermal Synthesis of metal oxide nanoparticles in supercritical water, Materials (Basel). 3 (2010) 3794–3817.
[23] K. Byrappa, T. Adschiri, Hydrothermal technology for nanotechnology, Prog. Cryst. Growth Char. Mater. 53 (2007) 117–166.
[24] U.M. Patil, J.S. Sohn, S.B. Kulkarni, S.C. Lee, H.G. Park, K.V. Gurav, J.H. Kim, S.C. Jun, Enhanced supercapacitive performance of chemically grown cobalt-nickel hydroxides on three-dimensional graphene foam electrodes, ACS Appl. Mater. Interfaces 6 (2014) 2450–2458.
[25] B. Wang, T. Zhu, H. Bin Wu, R. Xu, J.S. Chen, X.W. (David) Lou, Porous Co_3O_4 nanowires derived from long $Co(CO_3)_{0.5}(OH)\cdot 0.11H_2O$ nanowires with improved supercapacitive properties, Nanoscale 4 (2012) 2145.
[26] H.B. Wu, H. Pang, X.W. (David) Lou, Facile synthesis of mesoporous $Ni_{0.3}Co_{2.7}O_4$ hierarchical structures for high-performance supercapacitors, Energy Environ. Sci. 6 (12) (2013) 3619.
[27] L.P.F. Benício, R.A. Silva, J.A. Lopes, D. Eulálio, R.M.M. dos Santos, L.A. De Aquino, L. Vergütz, R.F. Novais, L.M. Da Costa, F.G. Pinto, J. Tronto, Layered double hydroxides : nanomaterials for applications in agriculture, Rev. Bras. Cienc. do Solo 39 (1) (2015) 1–13.
[28] Y. Ge, K. Kan, Y. Yang, L. Zhou, L. Jing, P. Shen, L. Li, K. Shi, Highly mesoporous hierarchical nickel and cobalt double hydroxide composite: fabrication, characterization and ultrafast NO_x gas sensors at room temperature, J. Mater. Chem. A 2 (2014) 4961–4969.
[29] J. Xiao, S. Yang, Bio-inspired synthesis of NaCl-type $Co_xNi_{1-x}O$ ($0 \leq x < 1$) nanorods on reduced graphene oxide sheets and screening for asymmetric electrochemical capacitors, J. Mater. Chem. 22 (2012) 12253.
[30] J. Yang, H. Cheng, R.L. Frost, Synthesis and characterization of cobalt hydroxy carbonate $Co_2CO_3(OH)_2$nanomaterials, Spectrochim. Acta Part A Mol. Biomol. Spectrosc. 78 (1) (2011) 420–428.
[31] S.K. Chang, Z. Zainal, K.B. Tan, N.A. Yusof, W.M.D.W. Yusoff, S.R.S. Prabaharan, Recent development in spinel cobaltites for supercapacitor application, Ceram. Int. 41 (2014) 1–14.
[32] D.S. Hall, D.J. Lockwood, S. Poirier, C. Bock, B.R. MacDougall, Raman and infrared spectroscopy of α and β phases of thin nickel hydroxide films electrochemically formed on nickel, J. Phys. Chem. A 116 (2012) 6771–6784.
[33] R.L. Frost, K.H. Bakon, S.J. Palmer, Raman spectroscopic study of synthetic reevesite and cobalt substituted reevesite $(Ni,Co)_6Fe_2(OH)_{16}(CO_3).4H_2O$, J. Raman Spectrosc. 41 (April 2009) (2010) 78–83.
[34] S.J. Palmer, T. Nguyen, R.L. Frost, Synthesis and Raman spectroscopic characterization of hydrotalcite with CO_3^{2-} and VO_3^- anions in the interlayer, J. Raman Spectrosc. 38 (2007) 1602–1608.
[35] X.Y. Liu, Y.Q. Zhang, X.H. Xia, S.J. Shi, Y. Lu, X.L. Wang, C.D. Gu, J.P. Tu, Self-assembled porous $NiCo_2O_4$ hetero-structure array for electrochemical capacitor, J. Power Sources 239 (2013) 157–163.
[36] X. Liu, D. Xu, D. Zhang, G. Zhang, L. Zhang, Superior performance of 3 D Co-Ni bimetallic oxides for catalytic degradation of organic dye: investigation on the effect of catalyst morphology and catalytic mechanism, Appl. Catal. B Environ. 186 (2016) 193–203.
[37] G.D. Park, Y.N. Ko, Y.C. Kang, Electrochemical properties of cobalt hydroxychloride microspheres as a new anode material for Li-ion batteries, Sci. Rep. 4 (2014) 5785.
[38] H. Sun, Q. Lin, M. Dong, Q. Wu, Structural transformation and electrochemical characterization of cobalt hydroxide carbonate nanostructures, Micro Nano Lett. 6 (2011) 190.
[39] C. Vaysse, L. Guerlou-Demourgues, C. Delmas, Thermal evolution of carbonate pillared layered hydroxides with (Ni, L) (L = Fe, Co) based slabs: grafting or non grafting of carbonate anions? Inorg. Chem. 41 (25) (2002) 6905–6913.
[40] C. Forano, T. Hibino, F. Leroux, C. Taviot-Guého, Chapter 13.1 layered double hydroxides, Dev. Clay Sci. 1 (Ii) (2006) 1021–1095.
[41] Y. Kim, E.S. Cho, S.J. Park, S. Kim, One-pot microwave-assisted synthesis of reduced graphene oxide/nickel cobalt double hydroxide composites and their electrochemical behavior, J. Ind. Eng. Chem. 33 (2016) 108–114.
[42] X. Sun, G. Wang, H. Sun, F. Lu, M. Yu, J. Lian, Morphology controlled high performance supercapacitor behavior of the Ni-Co binary hydroxide system, J. Power Sources 238 (2013) 150–156.
[43] L. Yu, N. Shi, Q. Liu, J. Wang, B. Yang, B. Wang, H. Yan, Y. Sun, X. Jing, Facile synthesis of exfoliated Co–Al LDH–carbon nanotube composites with high performance as supercapacitor electrodes, Phys. Chem. Chem. Phys. 16 (2014) 17936–17942.
[44] G. Rajeshkhanna, E. Umeshbabu, P. Justin, G. Ranga Rao, In situ fabrication of porous festucascoparia-like $Ni_{0.3}Co_{2.7}O_4$ nanostructures on Ni-foam: an efficient electrode material for supercapacitor applications, Int. J. Hydrogen Energy 40 (2015) 12303–12314.
[45] V. Gupta, T. Kusahara, H. Toyama, S. Gupta, N. Miura, Potentiostatically deposited nanostructured α-$Co(OH)_2$: a high performance electrode material for redox-capacitors, Electrochem. Commun 9 (2007) 2315–2319.
[46] Y. Gao, L. Mi, W. Wei, S. Cui, Z. Zheng, H. Hou, W. Chen, Double metal ions synergistic effect in hierarchical multiple sulfide microflowers for enhanced supercapacitor performance, ACS Appl. Mater. Interfaces 7 (2015) 4311–4319.
[47] L. Wang, X. Lu, Y. Ye, L. Sun, Y. Song, Nickel-cobalt nanostructures coated reduced graphene oxide nanocomposite electrode for nonenzymatic glucose biosensing, Electrochim. Acta 114 (2013) 484–493.
[48] Y. Tao, L. Ruiyi, L. Zaijun, L. Junkang, W. Guangli, G. Zhiquo, A free template strategy for the fabrication of nickel/cobalt double hydroxide microspheres with tunable nanostructure and morphology for high performance supercapacitors, RSC Adv. 3 (2013) 19416.
[49] Y. Tao, L. Ruiyi, Y. Tingting, L. Zaijun, Nickel/cobalt layered double hydroxide hollow microspheres with hydrangea-like morphology for high-performance supercapacitors, Electrochim. Acta 152 (2015) 530–537.
[50] A. Bello, O. Fashedemi, D.Y. Momodu, F. Barzegar, T.M. Masikhwa, M.J. Madito, F. Taghizadeh, J.K. Dangbegnon, N. Manyala, Electrochemical studies of microwave synthesised bimetallic sulfides nanostructures as faradaic electrodes, Electrochim. Acta 174 (2015) 778–786.
[51] A.L. Eckermann, D.J. Feld, J.A. Shaw, T.J. Meade, Electrochemistry of redox-active self-assembled monolayers, Coord. Chem. Rev. 254 (15–16) (2010) 1769–1802.
[52] E. Laviron, General expression of the linear potential sweep voltammogram in the case of diffusion less electrochemical systems, J. Electroanal. Chem.

Interfacial Electrochem. 101 (1979) 19–28.
[53] J. Xu, Y. Dong, J. Cao, B. Guo, W. Wang, Z. Chen, Microwave-incorporated hydrothermal synthesis of urchin-like $Ni(OH)_2$-$Co(OH)_2$ hollow microspheres and their supercapacitor applications, Electrochim. Acta 114 (2013) 76–82.
[54] D. Momodu, A. Bello, J. Dangbegnon, F. Barzeger, F. Taghizadeh, M. Fabiane, A.T.C. Johnson, N. Manyala, Solvothermal synthesis of NiAl double hydroxide microspheres on a nickel foam-graphene as an electrode material for pseudo-capacitors, AIP Adv. 4 (2014) 0–14.
[55] J. Chen, J. Xu, S. Zhou, N. Zhao, C.P. Wong, Amorphous nanostructured FeOOH and Co-Ni double hydroxides for high-performance aqueous asymmetric supercapacitors, Nano Energy 21 (2016) 145–153.
[56] G. Chen, S.S. Liaw, B. Li, Y. Xu, M. Dunwell, S. Deng, H. Fan, H. Luo, Microwave-assisted synthesis of hybrid $Co_xNi_{1-x}(OH)_2$nanosheets: tuning the composition for high performance supercapacitor, J. Power Sources 251 (2014) 338–343.
[57] K. Ma, J.P. Cheng, J. Zhang, M. Li, F. Liu, X. Zhang, Dependence of Co/Fe ratios in Co-Fe layered double hydroxides on the structure and capacitive properties, Electrochim. Acta 198 (2016) 231–240.
[58] X. Wang, J. Hao, Y. Su, F. Liu, J. An, J. Lian, A $Ni_{1-x}Zn_xS$/Ni foam composite electrode with multi-layers: one-step synthesis and high supercapacitor performance, J. Mater. Chem. A 4 (2016) 12929–12939.
[59] T.M. Masikhwa, M.J. Madito, D.Y. Momodu, J. K.Dangbegnon, O. Guellati, A. Harat, M. Guerioune, F. Barzegar, N. Manyala, High performance asymmetric supercapacitor based on CoAl-LDH/GF and activated carbon from expanded graphite, RSC Adv. 6 (2016) 46723–46732.
[60] Y. Liu, X. Teng, Y. Mi, Z. Chen, A new architecture design of Ni-Co LDHs-based pseudocapacitors, J. Mater. Chem. A 5 (2017) 24407–24415.
[61] A.A. Khaleed, A. Bello, J.K. Dangbegnon, F.U. Ugbo, F. Barzegar, D.Y. Momodu, M.J. Madito, T.M. Masikhwa, O. Olaniyan, N. Manyala, A facile hydrothermal reflux synthesis of $Ni(OH)_2$/GF electrode for supercapacitor application, J. Mater. Sci. 51 (12) (2016) 1–10.
[62] T.M. Masikhwa, J.K. Dangbegnon, A. Bello, M.J. Madito, D. Momodu, N. Manyala, Preparation and electrochemical investigation of the cobalt hydroxide carbonate/activated carbon nanocomposite for supercapacitor applications, J. Phys. Chem. Solid. 88 (2015) 60–67.
[63] J. Xiao, S. Yang, Sequential crystallization of sea urchin-like bimetallic (Ni, Co) carbonate hydroxide and its morphology conserved conversion to porous $NiCo_2O_4$ spinel for pseudocapacitors, RSC Adv. 1 (2011) 588–595.
[64] Y. Gao, L. Mi, W. Wei, S. Cui, Z. Zheng, H. Hou, W. Chen, Double metal ions synergistic effect in hierarchical multiple sulfide microflowers for enhanced supercapacitor performance, ACS Appl. Mater. Interfaces 7 (2015) 4311–4319.